TO: R. Browning

STATE OF NEVADA

AGENCY FOR NUCLEAR PROJECTS/ NUCLEAR WASTE PROJECT OFFICE

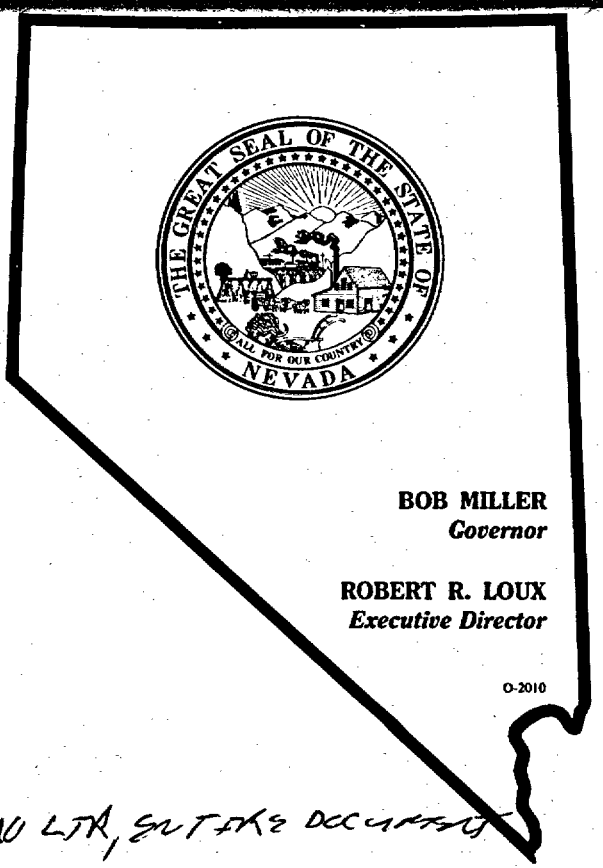

BOB MILLER
Governor

ROBERT R. LOUX
Executive Director

O-2010

NO LTR, SUPPORT DOCUMENTS

9008200074 900131
PDR WASTE
WM-11 PDC

Received w/Ltr Dated 1/31/90

STATE OF NEVADA
AGENCY FOR NUCLEAR PROJECTS
NUCLEAR WASTE PROJECT OFFICE

NWPO-TR-014-90

NUMERICAL SIMULATION OF GAS FLOW THROUGH UNSATURATED FRACTURED ROCK AT YUCCA MOUNTAIN, NEVADA

by

Clay A. Cooper
Water Resources Center
Desert Research Institute
University of Nevada System
Las Vegas and Reno, Nevada

January 1990

The Nevada Agency for Nuclear Projects/Nuclear Waste Project Office was created by the Nevada Legislature to oversee federal high-level nuclear waste activities in the state. Since 1985, it has dealt largely with the U.S. Department of Energy's siting of a high-level nuclear waste repository at Yucca Mountain in southern Nevada. As part of its oversight role, NWPO has contracted for studies of various technical questions at Yucca Mountain.

This study was funded by DOE grant number DE-FG08-85-NV10461.

ABSTRACT

Numerical analysis is used to identify the physical phenomena associated with barometrically driven gas (air and water vapor) flow through unsaturated fractured rock at Yucca Mountain, Nevada. Results from simple finite difference simulations indicate that for a fractured rock scenario, the maximum velocity of air out of an uncased 10 cm borehole is 0.002 m s^{-1}.

An equivalent porous medium (EPM) model was incorporated into a multiphase, multicomponent simulator to test more complex conceptual models. Results indicate that for a typical June day, a diurnal pressure wave propagates about 160 m into the surrounding Tiva Canyon hydrogeologic unit. Dry air that enters the formation evaporates water around the borehole which reduces capillary pressure. Multiphase countercurrent flow develops in the vicinity of the hole; the gas phase flows into the formation while the liquid phase flows toward the borehole. The effect occurs within 0.5 m of the borehole.

The amount of water vapor leaving the formation during 1 day is 900 cm^3. This is less than 0.1% of the total recharge into the formation, suggesting that the barometric effect may be insignificant in drying the unsaturated zone. However, gas phase velocities out of the borehole were on the order of 3 m s^{-1}, indicating that observed flow rates from wells along the east flank of Yucca Mountain were able to be simulated with a barometric model.

Table of Contents

ABSTRACT i
List of Figures iv
List of Tables vi
Chapter 1: INTRODUCTION 1
- Purpose 1
- Previous Work 2
- Setting 5
- Geology 7

Chapter 2: SINGLE-PHASE FLOW SIMULATIONS 11
- Conceptual Model 11
- Derivation of the One-Dimensional Gas Flow Equation 12
- Preliminary Numerical Simulations 16
  - Matrix Simulations 19
  - Fracture Simulations 21
- Topography Simulations 23

Chapter 3: MULTIPHASE FLOW SIMULATIONS: THEORY AND DEVELOPMENT 26
- Governing Equations 28
- Constitutive Relationships 29
- Equivalent Porous Medium 30
- Input Data 34
  - Rock Matrix Parameters 34
  - Fracture Parameters 35
  - Thermal Parameters 38
  - Material Properties of the Borehole 38
  - Boundary and Initial Conditions 39

Chapter 4: MULTIPHASE FLOW SIMULATIONS: APPLICATION 41
- Outward-Directed Pressure Gradient 42
- Inward-Directed Pressure Gradient 48
- Sinusoidal Pressure Boundary Condition 49
- Pressure Response 54

Chapter 5: SUMMARY AND CONCLUSIONS 56
REFERENCES 60
APPENDICES 64
A. Notation 64
B. GASFLO Source Listing 68
C. Modified relp.f subroutine in the TOUGH Computer Code 77

List of Figures

1.1 Location Map of Yucca Mountain. 6

1.2 Generalized stratigraphy at well UE-25 WT#17. 9

2.1 Cross-section of deep unsaturated zone showing mechanism for air movement. If $P_o > p$, air will move into the formation, causing well to "inhale." 12

2.2 Boundaries and boundary conditions for model described in Chapter 2. 15

2.3 Gas pressure vs. distance for 400 Pa (4 mb) pressure drop in well penetrating fractured rock. Simulation time is 2 days. 18

2.4 Flow rate of air out of borehole vs. time for 400 Pa pressure drop at well, matrix simulation. 20

2.5 Flow rate of air out of borehole vs. time for 400 Pa sinusoidal pressure disturbance at well, matrix simulation. 20

2.6 Flow rate of air out of borehole vs. time for 400 Pa pressure drop at well, fracture simulation. 22

2.7 Flow rate of air out of borehole vs. time for 400 Pa sinusoidal pressure disturbance at well, fracture simulation. 22

2.8 Flow rate of air out of borehole vs. time for 72 Pa pressure drop at 1000 m and 250 m, fracture simulation. 25

2.9 Flow rate of air out of borehole vs. time for 72 Pa pressure drop at 10 m and 5 m, fracture simulation. 25

3.1 Boundaries and boundary conditions for model described in Chapter 3. 27

3.2 Characteristic curve for Tiva Canyon hydrogeologic unit. 35

3.3 Log liquid relative permeability as a function of liquid saturation for Tiva Canyon hydrogeologic unit. 37

3.4 Log gas relative permeability as a function of liquid saturation for Tiva Canyon hydrogeologic unit. 37

3.5 Atmospheric pressure data for June 6, 1984 and sine function used as boundary condition for model. 40

4.1 Step change pressure condition for outward-directed pressure simulation. 42

4.2 Profile of liquid saturation, temperature, vapor pressure, and capillary pressure after 10 hours. Intrinsic permeability is 1.18×10^{-12} m^2. 43

4.3 Gas and liquid flow rates as a function of distance through the Tiva Canyon unit. Intrinsic permeability is 1.18×10^{-12} m^2. 45

4.4 Profile of liquid saturation as a function of distance at 10 and 20 hours simulation time. 45

4.5 Profile of liquid saturation, temperature, vapor pressure, and capillary pressure after 10 hours. Intrinsic permeability is 1.18×10^{-7} m^2. 47

4.6 Step change pressure condition for inward-directed pressure simulations. 48

4.7 Pressure history through Tiva Canyon 50 meters from borehole. Boundary condition at the borehole is equation 3.18. 49

4.8 Profile of pressure range at steady state for sine wave flow simulation. 51

4.9 Profile of liquid saturation range at steady state for simulation with sine wave pressure condition. 51

4.10 Gas velocity from borehole as a function of time for sine wave boundary condition. System is at steady state. 52

4.11 Pressure wave efficiency as a function of distance from borehole for three different intrinsic permeabilities. 55

4.12 Phase lag of pressure wave for three different permeabilities. 55

List of Tables

2.1 Input Data Required for GASFLO Simulations. 17

3.1 Summary of Differences Between Simulations in Chapter 2 and Chapters 3 and 4. 26

3.2 Model Parameters for Matrix. 34

3.3 Model Parameters for Fractures. 35

3.4 Thermophysical Properties and Their Values Used to Simulate a Borehole. 39

3.5 Initial Conditions Used in the Model. 39

4.1 Determination of Equivalent Volume of Water Leaving System During 1 Day. 53

Chapter 1

INTRODUCTION

Yucca Mountain, Nevada, has been proposed by the U.S. Department of Energy (U.S. DOE) to house the nation's first high-level radioactive waste repository. The repository would be located in the lower Topopah Spring Member of the Paintbrush Tuff (Sinnock et al., 1987) within the unsaturated zone (generally 400 to 700 meters total thickness). Significant gas (both air and water vapor) movement through this zone has been recognized since the early 1980's (Montazer and Wilson, 1984), and its implications are potentially great. If the waste package leaks, gaseous radionuclides (particularly ^{129}I and ^{14}C) may be rapidly transported upward to the atmosphere. Since 1985, the U.S. Geological Survey has collected data related to gas flow through rock beneath Yucca Ridge, flow that is induced by both topographic and barometric effects (Weeks, 1987; Kipp, 1987). However, this paper describes a model of barometrically induced gas flow on the eastern flank of the mountain, where some wells open to the atmosphere have been observed to "breathe" air. Flow in these wells is the result of a differential pressure gradient created at the interface of the borehole and the adjacent formation. The gradient is the result of fluctuations in atmospheric pressure with respect to air pressure in the formation. This effect causes gas to move in and out of the formation through the borehole. If flow is significant, sometimes an observer at the surface can feel air moving in or out of the borehole.

Purpose

To help assess the suitability of Yucca Mountain for waste disposal, it is important to understand the effects causing gas movement in the unsaturated zone. The ideal study would include both field and computational experiments;

however, because access to Yucca Mountain is limited, data collection for model validation is not currently feasible.

The purpose of this study is to explore several issues concerning the nature of unsaturated gas flow around a borehole: (1) Can a barometrically induced pressure gradient in an open borehole cause significant gas flow in the surrounding formation? If so, what is the surrounding pressure field around the borehole? (2) What is the range of gas velocities into and out of the borehole? (3) How much water vapor is leaving the system because of this flow, and can a drying scenario be established for the rock?

Previous Work

Prior to the 1980's, little modeling had been done on gas flow through unsaturated rock. Muskat (1937) presented the governing equations, in addition to compressible flow concepts and thermodynamics, derived from theory of flow in natural gas reservoirs. Aronofsky and Jenkins (1954) solved the flow equation for ideal gases and showed that production of an ideal gas could be approximated by liquid flow solutions. An early comprehensive work compiled by Carman (1956) linked together concepts such as viscous, diffusive (Knudsen, binary, thermal), two-phase, and turbulent flow.

Evans et al. (1961) developed a theory of binary diffusion in porous media from kinetic theory of gases. They developed a "dusty gas" model in which the porous medium is treated as a collection of large spheres (the "dust") and are actually another component of a multicomponent mixture. Evans et al. (1962) extended the theory from studying purely diffusive flow to diffusion in the presence of a pressure gradient. Recently, Thorstenson and Pollock (1989) reviewed and extended the theory, explaining that Fick's law does not adequately describe

gas flow in multicomponent mixtures, primarily when stagnant (zero flux) gases are present in the mixture. They demonstrated mathematically that for stagnant gases initially distributed equally throughout an unsaturated zone, concentration gradients can be created strictly through transport of the mobile components.

With respect to thermally induced moisture flow, Philip and de Vries (1957) developed a theory based on coupling between mass and energy. They defined four moisture dependent diffusivities introduced with the equations. At high moisture contents, flow is dominated by liquid diffusivity, while at low moisture, flow is controlled by vapor diffusivity. Sophocleous (1979) reviewed and modified Philip and de Vries (1957) model by reformulating the equations in terms of pressure head, rather than moisture content. He redefined the thermal liquid water diffusivity (originally defined by Philip and de Vries, 1957) and determined that thermal gradients become the dominant driving force at low moisture contents. Sophocleous (1979) also determined that the coupling of energy with flow has little effect on the temperature distribution in soils, but significantly alters evaporation, and therefore moisture fluxes. Milly (1982) extended Philip and de Vries work by including hysteresis in the formulation and development of a numerical code.

The theory of water table fluctuations in both confined and unconfined systems as a result of barometric pressure fluctuations was investigated by Jacob (1940), Peck (1960), Norum and Luthin (1968), Turk (1975), and Weeks (1979). Though none of these workers studied the gas phase intrinsically, much of the theory can be modified to explain gas flow in the unsaturated zone. Weeks' (1979) explanation of water level fluctuations in deep unconfined aquifers as a result of barometric pressure fluctuations is modified and used as the conceptual model to explain gas flow in these same systems in this report.

Kemper et al. (1986) presented some concepts concerning advective transport of gases through fractured basalt in Idaho. During winter, air and water vapor were blown out of a dry well penetrating the basalt. In summer, the reverse occurred and the low relative humidity atmospheric air was sucked into the borehole. They determined that in addition to flow being controlled seasonally, it was also affected by daily barometric pressure fluctuations.

In relation to Yucca Mountain, Weeks (1987) discussed some general concepts regarding air moving in and out of wells USW UZ-6 and USW UZ-6s, along the ridge of Yucca Mountain. He identified both a barometric and a topographic effect inducing air flow in the deep unsaturated zone. Kipp (1987) ran computer simulations using data from Weeks (1987) and determined that seasonal variations in surface air temperature can induce air circulation in the unsaturated zone.

Knapp (1987) developed a kinematic wave equation for advective transport of ^{14}C in the gas phase that takes into account decay of ^{14}C and isotope exchange with liquid bicarbonate. He then solved the equation analytically for a single release scenario at Yucca Mountain.

Until recently, computer codes capable of simulating multiphase, "strongly" heat-driven flow had not been developed. The models developed by Philip and de Vries (1957), Sophocleous (1979), and Milly (1982) consider gas flow as only a diffusive process. Updegraff and Bonano (1988) evaluated three strongly heat-driven codes, TOUGH (Pruess, 1987), NORIA (Bixler, 1985), and PETROS (Hadley, 1985). All solve nonisothermal mass (both liquid and gas) and energy transport equations. After running sample problems on each code, Updegraff and Bonano (1988) made recommendations for improvement based upon strong and weak characteristics of each code.

Of historical interest, possibly the first published report of a "breathing" well was made by Fairbanks (1896) who noted that a water well in San Luis Obispo County, California, intermittently inhaled air and exhausted natural gas. The gas was of sufficient quality to burn in incandescent lamps, and was used to light buildings on a nearby ranch. He noted that the well intermittently exhausted gas and inhaled air during periods of "settled" weather, with each period lasting about 3 hours. During stormy weather, the well exhausted gas sometimes for as long as 24 hours. Fairbanks (1896) correctly identified barometric pressure as the driving mechanism, but was unable to explain the physics of the system.

Setting

Yucca Mountain is located in the southern Basin and Range geologic province (Figure 1.1). The terrain is rugged, ranging in elevation from 1475 m along the crest to 1015 m at Jackass Flats, to the east. It is composed primarily of ash-flow and ash-fall tuffs, as the result of extensive Miocene volcanic activity (Montazer and Wilson, 1984, p. 5). The area is dissected by a series of north trending fault block ridges, with dips 5° to 10° to the east.

Climate in the area is arid; precipitation averages 150 mm yr^{-1}, three-fourths of which falls between October and April. Occasional snow falls on the ridges; however, the climate is generally too warm for it to last more than a few days. All streams in the area are ephemeral. They flow for short durations after intense storms or rapid snowmelt. Most of the small washes drain east into Fortymile Wash.

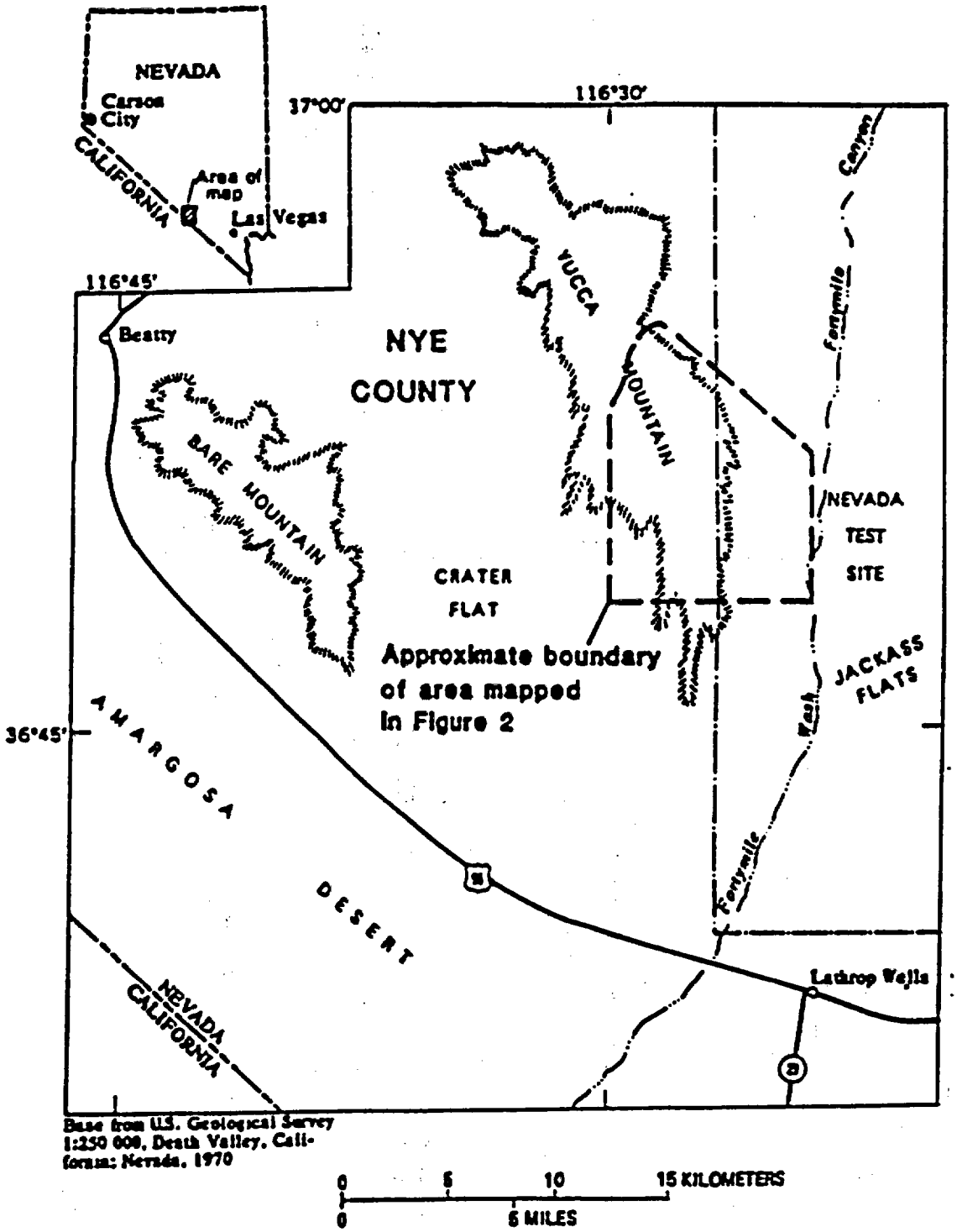

Figure 1.1. Location of Yucca Mountain, Nevada (from Montazer and Wilson, 1984).

Geology

Gas flow in this study is modeled in relation to borehole UE-25 WT#17, just west of Busted Butte Road, in area 25 of the Nevada Test Site. It has been noted in various Desert Research Institute (Reno, Nevada) monthly reports in 1987 and 1988 to "breathe" air. The surface coordinates of UE-25 WT#17 are N 748,420', E 566,212' in area 25 of the Nevada Test Site (Fenix and Scisson Drilling and Mining Summary through December, 1987; no document number). Surface elevation is 1124 m above mean sea level. It is far enough from the ridge of Yucca Mountain (3.2 km) that no topographic effect is expected to drive unsaturated gas flow.

Rock stratigraphic units at Yucca Mountain have been described by Scott et al. (1983), Scott and Castellanos (1984), Spengler and Chornack (1984), and Spengler et al. (1981). However, far more important to a study of this nature is a delineation of stratigraphy based upon physical rock properties. This allows division of the strata into hydrogeologic units, as opposed to the more typical rock stratigraphic units. Because porous media fluid flow is a physical process, a stratigraphy based upon hydrologic and hydraulic characteristics such as grain density, intrinsic permeability, porosity, and fracture density is needed. Correlations between lithostratigraphic and hydrogeologic units are presented in Montazer and Wilson (1984, p. 12,13), Ortiz et al. (1985, p. 44), and Scott et al. (1983, p. 301). From these stratigraphic columns, one gets a sense of how lithostratigraphic and hydrogeologic units correlate.

A lithostratigraphic column for UE-25 WT#17 based upon petrologic characteristics is presented in Muller and Kibler (1985, p. 28). Delineation of physical-property stratigraphy in this well has not been accomplished. In this report, it is assumed that rock stratigraphy and physical-property stratigraphy correlate

exactly. In descending order from the land surface, the hydrogeologic units at UE-25 WT#17 are the Tiva Canyon, Topopah Spring, Calico Hills zeolitic, and Prow Pass (Figure 1.2). The term "unit" in this report is synonymous with "hydrogeologic unit" and is used for brevity.

The Tiva Canyon unit extends from the land surface to a depth of 75 m. Within the study area, it dips 5° to 10° eastward (Montazer and Wilson, 1984, p. 14). Fracture density is high, around 20 fractures m^{-3} (Sinnock et al., 1987, p. 7825; Montazer and Wilson, 1984). Most of the permeability is due to fracture density, as matrix permeability is low (Montazer and Wilson, 1984, p. 14; Sinnock et al., 1987, p. 7825).

Below the Tiva Canyon unit is the Topopah Spring unit. (The Paintbrush Tuff unit, present over much of Yucca Mountain, is absent at UE-25 WT#17.) The Topopah Spring is the thickest unit (225 m) in the unsaturated zone at UE-25 WT#17. The unit has physical characteristics similar to the Tiva Canyon: it is densely welded and highly fractured with low matrix permeability (Montazer and Wilson, 1984, p. 15). In some locations, the Topopah Spring unit has isolated gas-filled cavities (Montazer and Wilson, 1984, p. 15; Scott et al., 1983, p. 293). The effect of these cavities on the hydrologic properties of the rock is not well understood; however, because many of them are isolated from each other and the surrounding rock matrix, one probable effect is a marked contrast between total and effective porosity.

Beneath the Topopah Spring unit is the Calico Hills zeolitic unit (Muller and Kibler, 1985; Montazer and Wilson, Figure 4, p. 18). This unit is a nonwelded to partially welded tuff that has been devitrified. Alteration products are dominantly zeolites, which probably formed when the water table was higher and the formation was saturated. Other alteration products include clay and calcite.

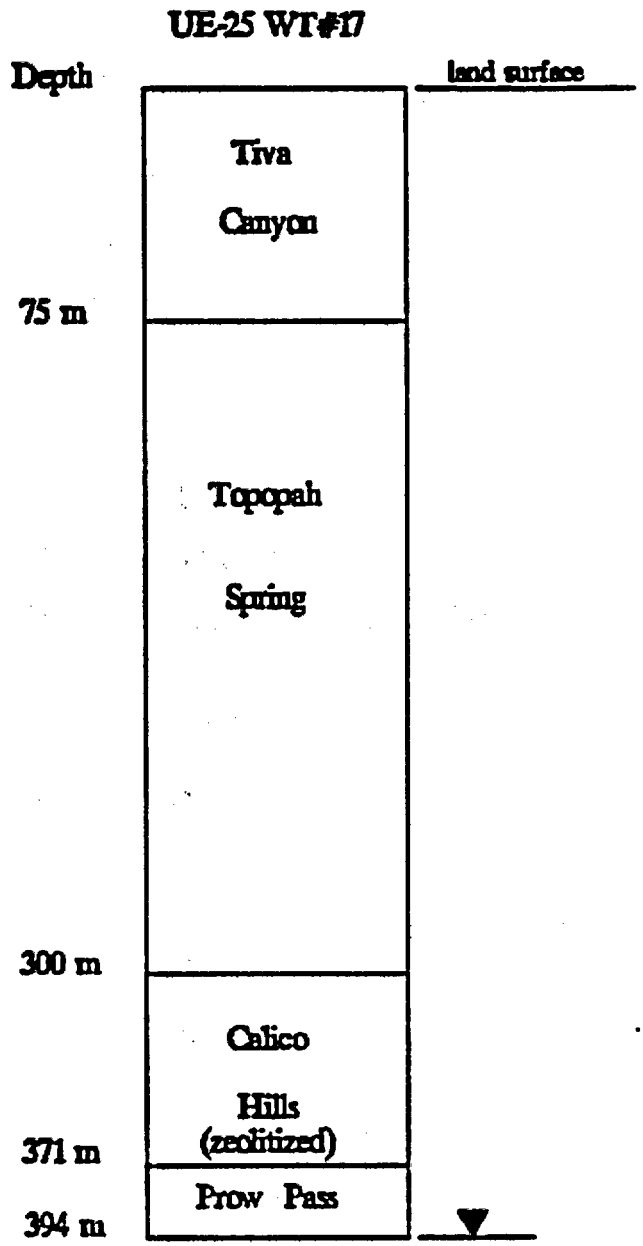

Figure 1.2. Generalized stratigraphy at well UE-25 WT#17.

Beneath the Calico Hills zeolitic unit lies the Prow Pass welded unit (Muller and Kibler, 1985, p. 28; Ortiz et al., 1985, p. 44). Only a few cores of this unit have been taken, so little is known about its hydrologic properties. It is assumed that this is the lowermost unit in the unsaturated zone around UE-25 WT#17.

Chapter 2
SINGLE-PHASE FLOW SIMULATIONS

Conceptual Model

Movement of gas in a deep unsaturated zone around an open borehole is the result of a differential pressure gradient created at the interface of the hole and the adjacent formation. The air pressure gradient can be the result of several physical phenomena such as wind blowing above the land surface creating a venturi effect in the well, barometric pressure gradients caused by passing storm fronts, earth tides, and diurnal barometric pressure fluctuations. The driving mechanism in this model only considers daily barometric pressure fluctuations. The term "gas" includes all gas present in the unsaturated zone: air, water vapor, CO_2, CH_4, N_2, Ar, etc.

The conceptual flow model is developed primarily from Weeks' (1979) model which explains water table fluctuations in deep unsaturated zones. Gas flow will occur only if a well penetrating a deep unsaturated zone is uncased, or has a slotted screen, through some part of the zone (Figure 2.1). Initially air pressure in the well is the same as that in the formation. An atmospheric pressure disturbance is transmitted instantaneously to the air in the well; however, the pressure wave is attenuated as it passes down through the unsaturated zone. This is caused by compression of the gas and friction with the porous medium as the pressure wave passes through the zone. The result of these two paths taken by the wave is a pressure imbalance created at the borehole/formation interface. If the atmospheric pressure disturbance is less than the original formation pressure, the pressure gradient will be directed from the formation into the well, causing vadose zone gas to be blown out of the well. If the pressure disturbance is greater than

the original formation pressure, the situation is opposite and air will be drawn into the formation. Either situation alters the pressure and velocity field around the well. The degree of differential pressure at the borehole determines the pressure field in the surrounding well. The relative humidity difference between air in the borehole and air in the formation creates changes in the water balance in the formation.

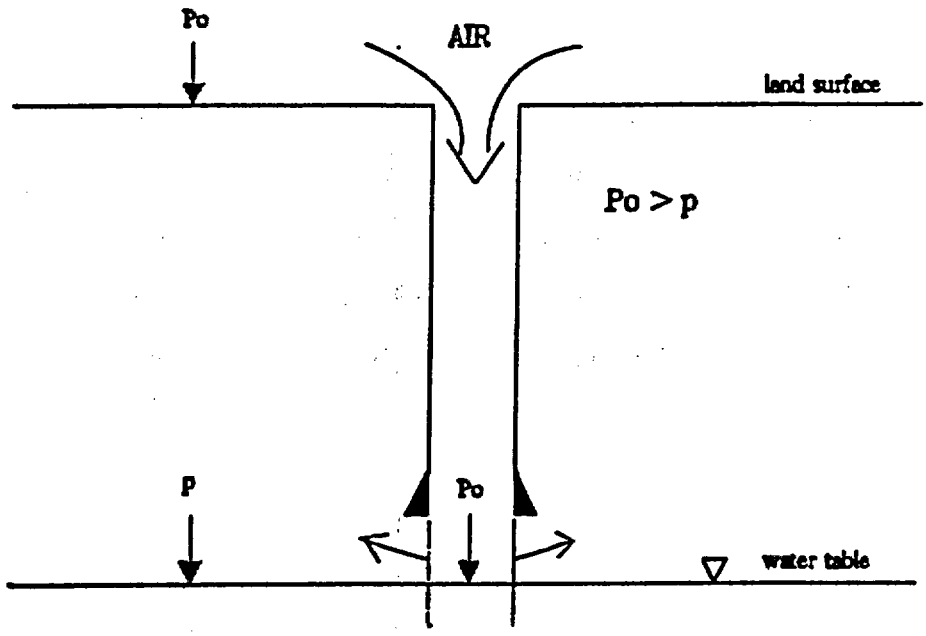

Figure 2.1. Cross-section of deep unsaturated zone showing mechanism for air movement. If $P_o > p$, air will move into the formation, causing well to "inhale."

Derivation of the One-Dimensional Gas Flow Equation

A finite difference program (GASFLO) was written to solve some one-dimensional, single-phase flow problems. The purpose was to gain understanding for simple flow fields when a pressure disturbance is created in the borehole. These findings were then used as an aid in designing the numerical simulations

with the TOUGH program, which incorporates partial saturation and thermal effects.

The model is also used to test the following hypothesis. Can measured velocities from borehole USW UZ-6 (Weeks, 1987) be simulated with a barometric model? These are the only air velocities measured near the study area; hence the only velocities to compare simulation results. A topographic model is also discussed and the code is used to see if measured velocities can be duplicated numerically with this model.

Derivation of the governing equation begins with equations of flux, state, and balance. The flux equation for one-dimensional radial flow (no elevation potential) is

$$q = -\frac{k}{\mu}\frac{\partial P}{\partial r} \tag{2.1}$$

where q is darcy velocity, k is intrinsic permeability, μ is dynamic viscosity, P is pressure, and r is radius.

The state equation is for ideal gases

$$PV = \eta RT \tag{2.2}$$

where V is volume, η is moles of the gas, R is the universal gas constant, and T is temperature. Knowing that

$$m = M\eta \tag{2.3}$$

where m is mass of a gas, and M is its molecular weight, gives

$$\frac{m}{V} = \rho = \frac{PM}{RT} \tag{2.4}$$

Finally the mass balance equation in radial coordinates (Bird et al., 1960, p. 83)

$$\theta_g \frac{\partial \rho}{\partial t} = -\frac{1}{r}\frac{\partial}{\partial r}(\rho r q) \tag{2.5}$$

where θ_g is volumetric gas content and ρ is mass density of the gas. Substitution of (2.1) and (2.4) into (2.5)

$$\theta_g \frac{\partial}{\partial t}\left(\frac{PM}{RT}\right) = \frac{1}{r}\frac{\partial}{\partial r}\left(\frac{PM}{RT} r \frac{k}{\mu}\frac{\partial P}{\partial r}\right) \tag{2.6}$$

and for M, R, T, k, and μ constant (at low pressure, μ is independent of pressure, Bird et al., 1960, p. 24; Baehr et al., 1989, p. 24)

$$\theta_g \frac{\partial P}{\partial t} = \frac{1}{r}\frac{k}{\mu}\frac{\partial}{\partial r}\left(rP\frac{\partial P}{\partial r}\right) \tag{2.7}$$

Recognizing that

$$P\frac{\partial P}{\partial r} = \frac{1}{2}\frac{\partial P^2}{\partial r} \tag{2.8}$$

and using the chain rule gives

$$\frac{2\theta_g \mu}{k}\frac{\partial P}{\partial t} = \frac{\partial^2 P^2}{\partial r^2} + \frac{1}{r}\frac{\partial P^2}{\partial r} \tag{2.9}$$

Since $\frac{\partial P}{\partial t} = \frac{1}{2P}\frac{\partial P^2}{\partial t}$, the governing equation becomes

$$\frac{\partial^2 P^2}{\partial r^2} + \frac{1}{r}\frac{\partial P^2}{\partial r} = \frac{\theta_g \mu}{kP}\frac{\partial P^2}{\partial t} \tag{2.10}$$

The following boundary and initial conditions are used in the model (Figure 2.2):

$$P(0,t) = P_A \tag{2.11}$$

$$P(R,t) = P_0 \tag{2.12}$$

$$P(r,0) = P_0 \tag{2.13}$$

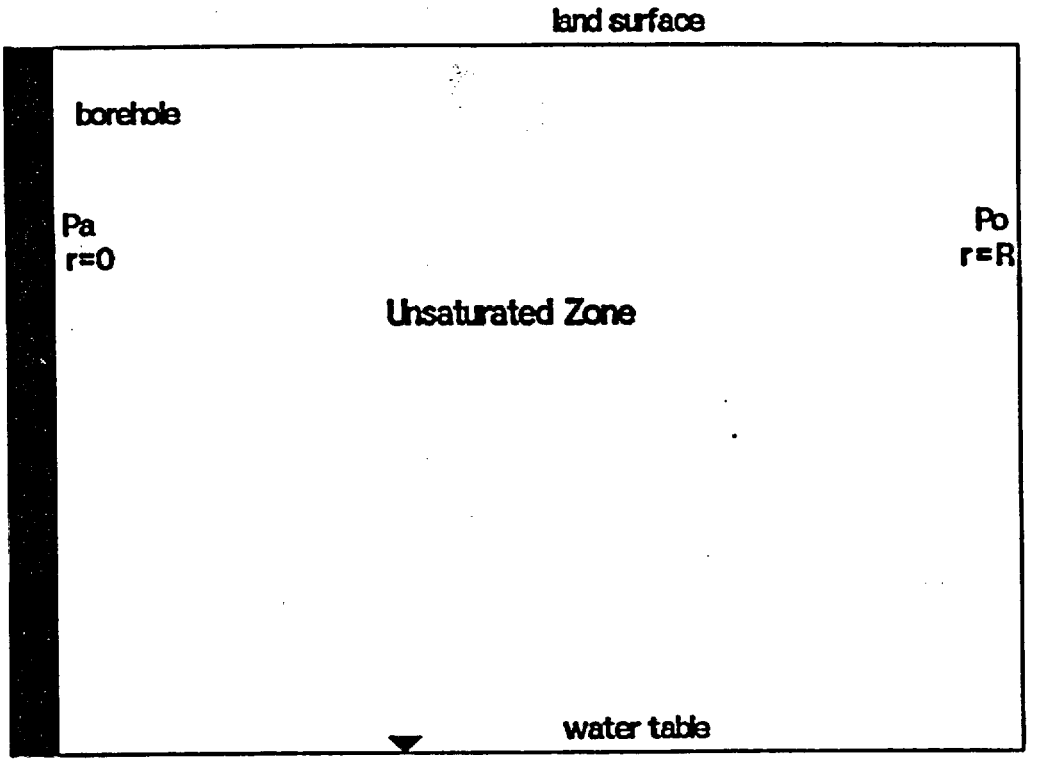

Figure 2.2. Boundaries and boundary conditions for model described in Chapter 2.

Because compressibility $(\frac{1}{P})$ is dependent upon pressure, the equation is non-linear, and no unique analytical solution exists. Equation (2.10) with its corresponding boundary conditions was solved using a Crank-Nicolson time stepping procedure. The corresponding difference equations are (where $U = P^2$)

$$\frac{\partial^2 U}{\partial r^2} = \frac{\left(U_{j+1}^{n+1} - 2U_j^{n+1} + U_{j-1}^{n+1}\right) + \left(U_{j+1}^{n} - 2U_j^{n} + U_{j-1}^{n}\right)}{2(\Delta r)^2} \tag{2.14}$$

$$\frac{\partial U}{\partial r} = \frac{U_{j+1}^{n+1} - U_{j-1}^{n+1} + U_{j+1}^{n} - U_{j-1}^{n}}{4\Delta r} \tag{2.15}$$

$$\frac{\partial U}{\partial t} = \frac{U_j^{n+1} - U_j^{n}}{\Delta t} \tag{2.16}$$

GASFLO handles prescribed pressure boundary conditions only, which is suitable for this study because all of the problems were of this type. Input constants are intrinsic permeability, dynamic viscosity, volumetric gas content, and formation thickness. The initial condition (pressure) is prescribed at each node. The source code listing is in Appendix B.

Preliminary Numerical Simulations

The program solves one-dimensional, transient, radial gas flow. Since the entire unsaturated zone at UE-25 WT#17 was modeled, volumetric gas contents and permeabilities for all hydrogeologic units were vertically averaged to determine composite k and θ_g values for the unsaturated zone.

Vertically averaged intrinsic permeability is determined using the concept of "equivalent hydraulic conductivity" in layered media (McWhorter and Sunada, 1977, p. 85). Flow is assumed horizontal to the bedding. A composite intrinsic permeability can be determined from

$$\bar{k} = \frac{\sum_{i=1}^{j} k_i b_i}{b_t} \tag{2.17}$$

where $\bar{k}$ is the averaged intrinsic permeability, k_i is each unit's intrinsic permeability, b_i is the thickness of each unit, and b_t is the total thickness of the unsaturated zone. The subscript i means that the values are summed for each individual unit.

Vertically averaged gas content ($\bar{\theta}_g$) is determined using

$$\bar{\theta}_g = \frac{\sum_{i=1}^{j} \theta_{g_i} b_i}{b_t} \tag{2.18}$$

where θ_{g_i} is the volumetric gas content of each hydrogeologic unit. θ_{g_i} is determined through a relationship between porosity and moisture saturation. θ_g for a given hydrogeologic unit is determined from (Hillel, 1980, p. 14)

$$\theta_g = n(1 - S_l) \tag{2.19}$$

where n is the porosity and S_l is the liquid saturation.

Because two of the hydrogeologic units are fractured (Tiva Canyon and Topopah Spring), two types of simulations were run: (1) simulations in which only the matrix properties were used in calculate $\bar{k}$ and $\bar{\theta}_g$ and (2) simulations in which fracture properties were used to calculate the same variables. Details are discussed below. Table 2.1 presents the input data for both matrix and fracture simulations. In all simulations, the gas phase properties are those of dry air.

TABLE 2.1. Input Data Required for GASFLO Simulations.

	Matrix Simulations		Fracture Simulations	
μ [a] kg m^{-1}s^{-1}	$\bar{\theta}_g$ [b]	$\bar{k}$ [c] m^2	$\bar{\theta}_g$ [b]	$\bar{k}$ [c] m^2
1.84E-5	.0249	2.01E-17	.00565	9.06E-13

[a] From CRC Handbook of Chemistry and Physics.
[b] Calculated from (2.18) and (2.19) using data from Sinnock et al. (1987, p. 7825).
[c] Calculated from (2.17) using data from Sinnock et al. (1987, p. 7825).

An arbitrary simulation time of 2 days was chosen. The first problem was to determine the extent of the flow system that could be used in all simulations. Not surprisingly, it was determined that a pressure disturbance created at a borehole travels fastest through fractured rock. A 400 Pa (4 mb) pressure wave propagates 880 m after 2 days (Figure 2.3). Therefore, a 1000 m system radius was used to

prevent the outer boundary from interfering with the solution domain. With this system the two types of simulations were run.

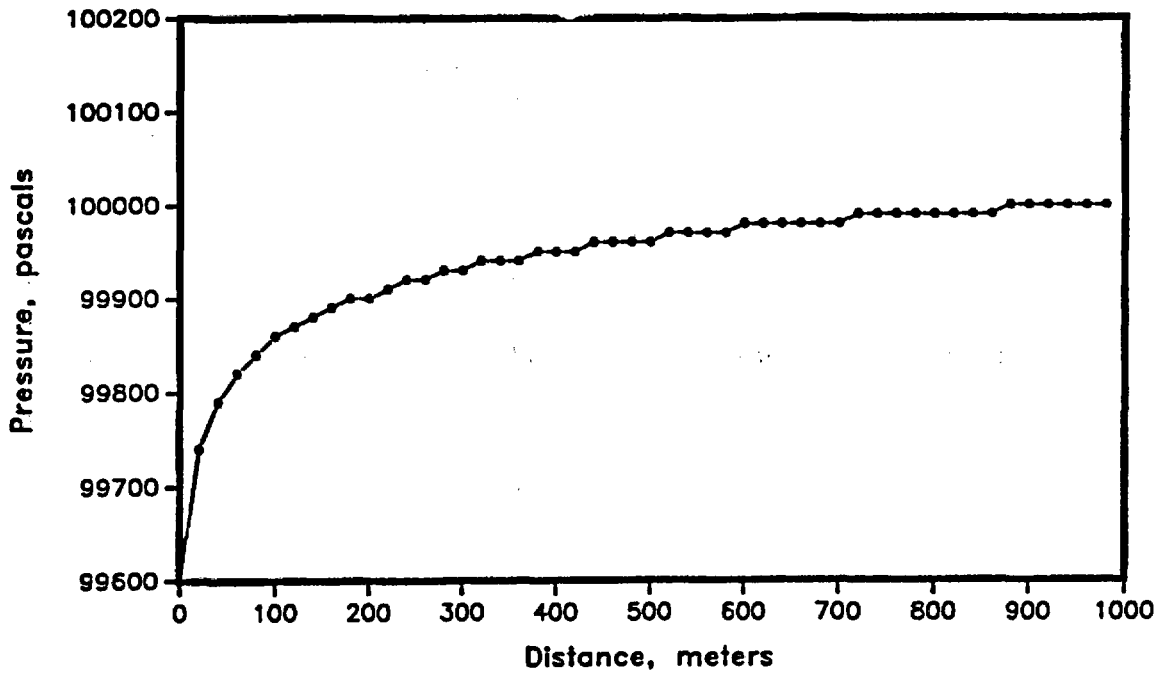

Figure 2.3. Gas pressure vs. distance for 400 Pa (4 mb) pressure drop in well penetrating fractured rock. Simulation time is 2 days.

The velocity of air escaping from the borehole was computed in each simulation. This velocity (V) is calculated by

$$V = \frac{Q}{A} = \frac{2\pi r q b_t}{\pi r^2 \overline{\theta}_g} \tag{2.20}$$

where Q is the volumetric discharge of air ($m^3\ s^{-1}$), A is the cross sectional area of the borehole, r is the borehole radius, q is the specific discharge into the borehole ($m\ s^{-1}$), $\overline{\theta}_g$ is the gas saturation, and b_t is the unsaturated zone thickness. This velocity assumes frictionless, incompressible flow up the borehole. The value was then compared with a measured flow rate from USW UZ-6 (along the

crest of Yucca Mountain) to determine if this measured value could be simulated with barometrically induced flow.

MATRIX SIMULATIONS These flow simulations were run with pressure prescribed at the borehole. Two types of simulations were run, however, each with the pressure boundary condition handled differently. The first was prescribed constant pressure, while the second was prescribed sinusoidally time-varying pressure. The borehole boundary condition is from Church et al. (1987). The pressure is assumed to fluctuate 400 Pa daily. For constant pressure simulations, 10^6 Pa was assumed in the formation, while an instantaneous pressure drop of 400 Pa was applied at the borehole. Figure 2.4 shows the flow rate of air out of the borehole vs. time assuming matrix-only rock properties. For a 400 Pa initial pressure drop in the borehole, the flow rate of air out the borehole is initially 1.37×10^{-5} m s^{-1}. After 2 days of simulation, the flow rate out the borehole approached 1.04×10^{-5} m s^{-1} as the system stabilized. Weeks (1987) reports wintertime flow rates of 3 m s^{-1} from USW UZ-6 on the ridge of Yucca Mountain. The simulated flow velocities are 5 orders of magnitude less than Weeks' (1987) measured values. This simple matrix flow model fails to reproduce observed values.

Matrix simulations were also run by prescribing a time-varying sinusoidal pressure boundary condition at the borehole. The initial condition is the same as that used in the constant pressure simulation; however, a diurnal, sinusoidal barometric pressure fluctuation is assumed at the borehole using

$$P(t) = P_0 + A \sin(\frac{2\pi t}{\tau}) \tag{2.21}$$

where P and P_0 are the updated and initial pressures at the well, respectively

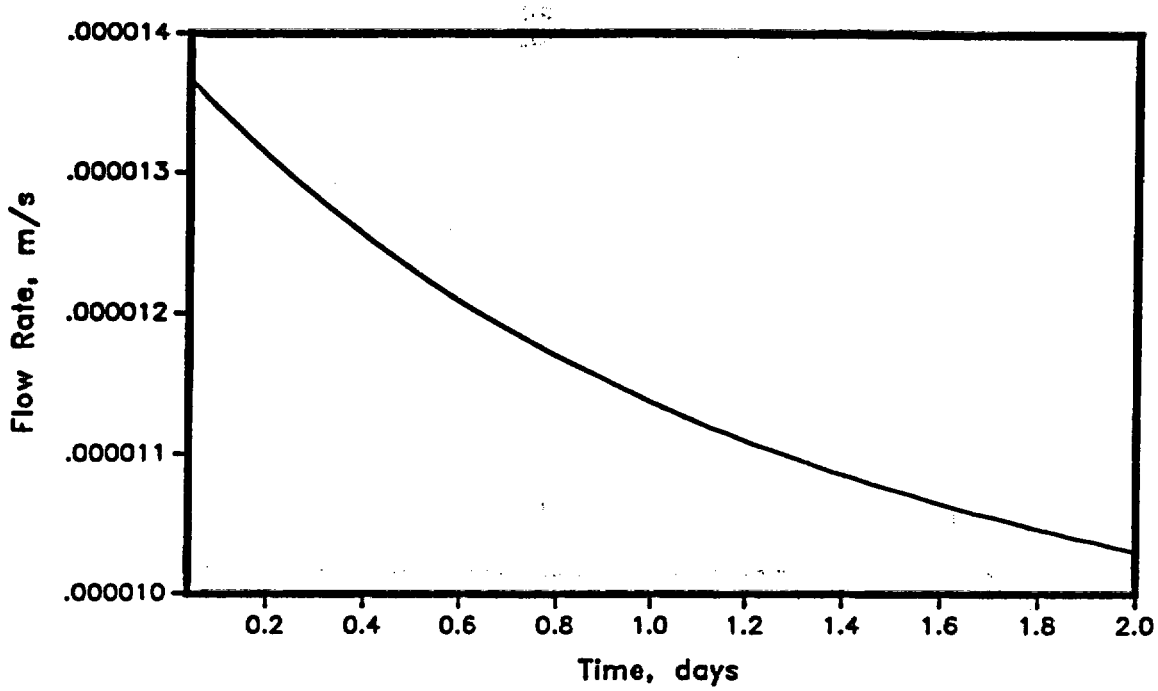

Figure 2.4. Flow rate of air out of borehole vs. time for 400 Pa pressure drop at well, matrix simulation.

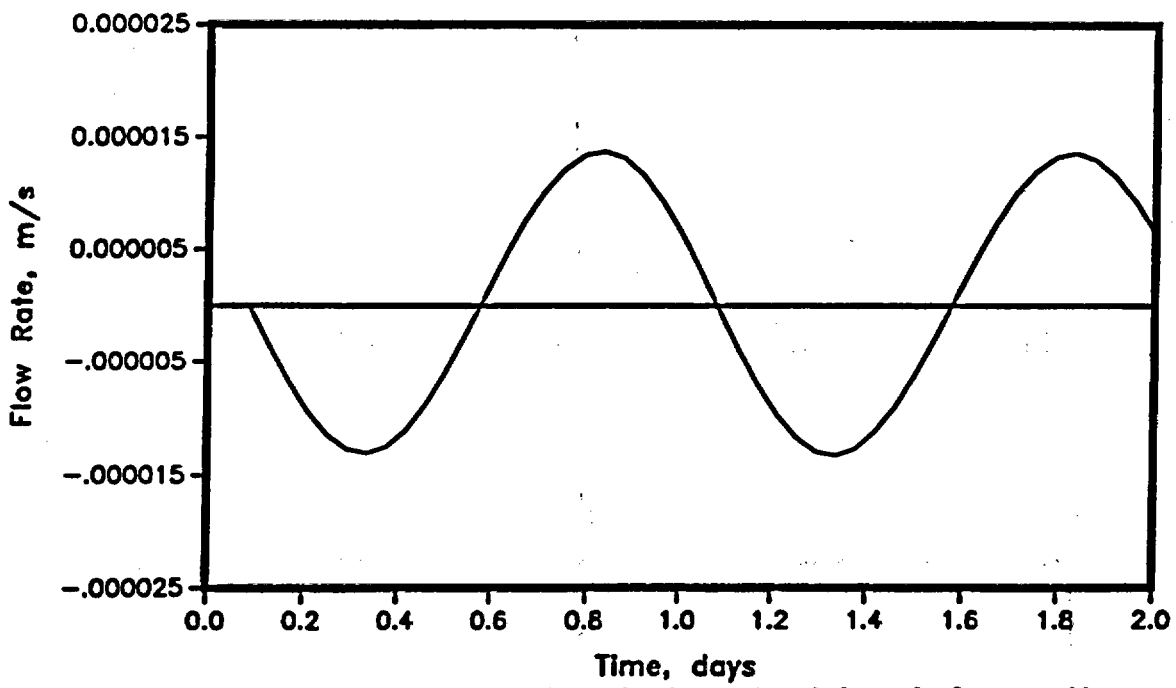

Figure 2.5. Flow rate of air out of borehole vs. time for 400 Pa sinusoidal pressure disturbance at well, matrix simulation.

(P_0 = 100,000 Pa), A is the amplitude of the sine wave (400 Pa), t is time, and τ is the wave period (1 day). In this simulation, the well alternately exhaled and inhaled air at flow rates between $\pm 1.2 \times 10^{-5}$ m s^{-1} (Figure 2.5). These flow rates are of the same order of magnitude as those for the previous case.

FRACTURE SIMULATIONS A second set of simulations were run that incorporated fracture properties of the Tiva Canyon and Topopah Spring hydrogeologic units. These units are heavily fractured, ranging from 20 to 40 fractures m^{-3} (Sinnock et al., 1987, p. 7825). As in the previous simulations, equations (2.17) and (2.18) were used to compute $\bar{k}$ and $\bar{\theta}_g$. In these units however, only the fracture properties (k_f, n_f, θ_f) were used to compute $\bar{k}$ and $\bar{\theta}_g$. No matrix properties of the Tiva Canyon or Topopah Spring units were included. This is because the conceptual model for fractured rock is that of Wang and Narasimhan (1985) which describes fractures in unsaturated rock as dry (and contributing to gas flow) while liquid is in the matrix. For fractured Yucca Mountain tuffs, fracture permeability is four orders of magnitude larger than the matrix permeability. If the fractures are dry, which this model assumes, then gas flow is controlled by fractures, and is negligible through the matrix. Input data for the fracture simulations is in Table 2.1.

Using data from Sinnock et al. (1987), $\bar{k}$ and $\bar{\theta}_g$ were re-computed using equations (2.17) and (2.18). Simulations were then run using the same boundary and initial conditions as the matrix simulations.

Air flow rates out the borehole for both the step change and sinusoidal borehole pressure disturbance simulations are shown in Figures 2.6 and 2.7. Figure 2.6 shows an initial velocity of 5.0×10^{-3} m s^{-1} that stabilizes to 2.5×10^{-3} m s^{-1} after 2 days of simulation. Compared to the corresponding matrix

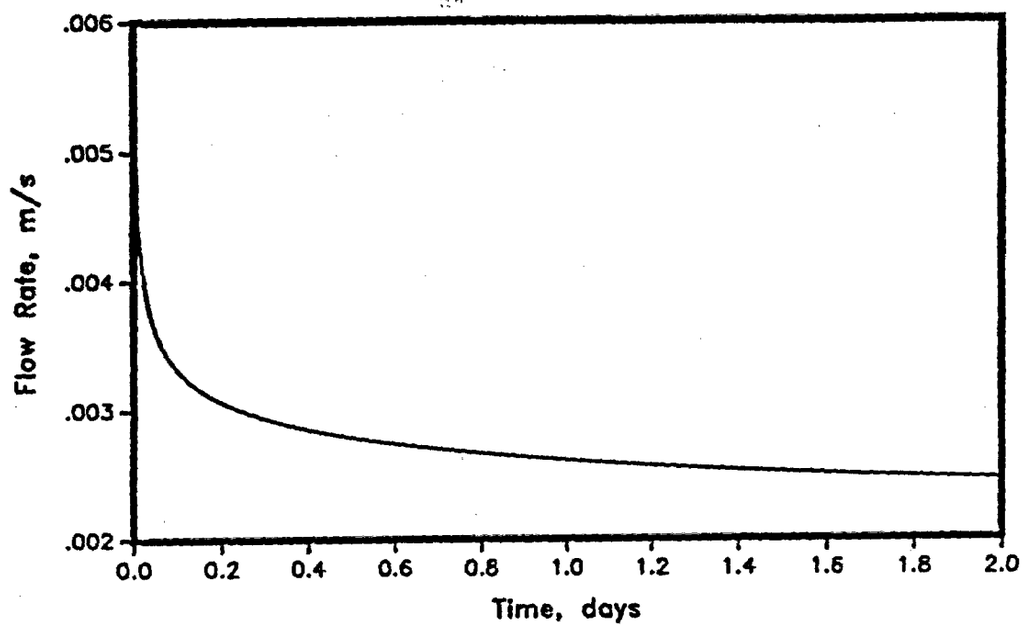

Figure 2.6. Flow rate of air out of borehole vs. time for 400 Pa pressure drop at well, fracture simulation.

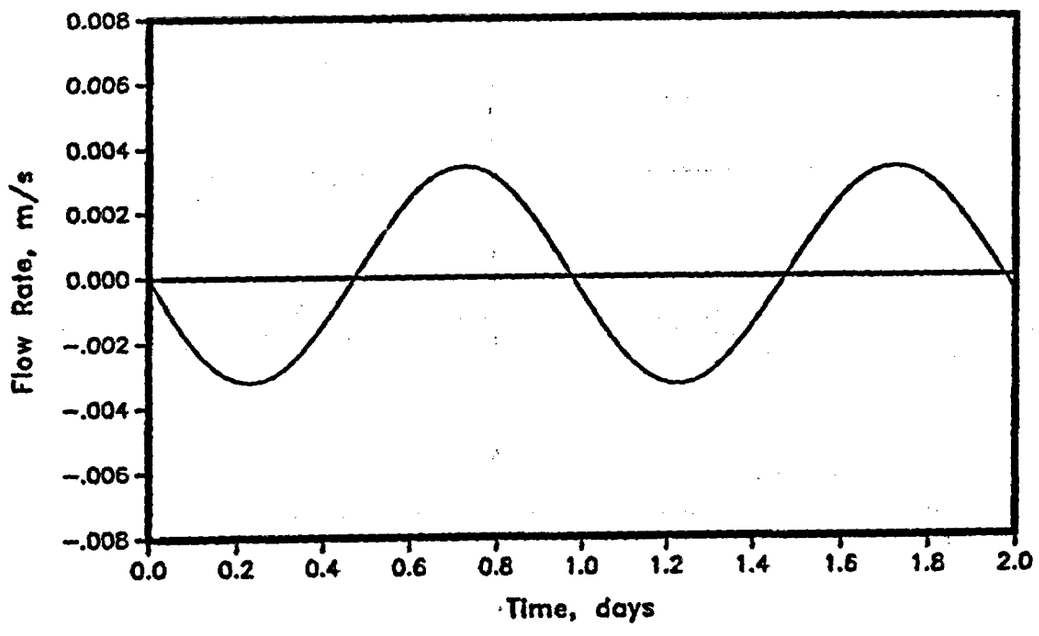

Figure 2.7. Flow rate of air out of borehole vs. time for 400 Pa sinusoidal pressure disturbance at well, fracture simulation.

simulation, flow rate out the borehole increases 2 orders of magnitude.

Air flow rates of the same order of magnitude resulted from the sinusoidal pressure simulations (Figure 2.7). Flow rates ranged from $\pm 3.6 \times 10^{-3}$ m s^{-1}, meaning that the well alternately inhaled and exhaled air. The boundary condition at the borehole is the same as that used in the matrix simulations, equation (2.21). For both types of fracture simulations (step change and sinusoidal boundary condition), the borehole flow rates are still 3 orders of magnitude less than those measured by Weeks (1987). The largest flow rates simulated are on the order of 10^{-3} m s^{-1} (<0.1 mile per hour) and are therefore undetectable. Not surprisingly, gas flow rates are greatly increased when the model is formulated with fracture parameters, as opposed to matrix parameters.

Topography Simulations

Simulations were run in which the topographic effect explained by Weeks (1987) was modeled. Conceptually, if the temperature in a mountain is different than the outside air temperature along the face of the mountain, a pressure imbalance will be generated across the face. This is the result of different air densities inside and outside the mountain. The mathematical model visualizes a series of concentric cylinders with a borehole in the center. A pressure gradient is applied across the outer face of the cylinder, analogous to a pressure gradient created along the face of a mountain as a result of a dense column of air. This model therefore applies a pressure gradient across the two outermost elements, and assumes formation and borehole pressures are initially equal.

Formation properties are the same as in the fracture model described above. Computer runs were made for a system radius of 1000, 250, 10, and 5 meters. As the radius becomes smaller, velocities increase towards the borehole. The purpose

of these simulations is to determine if the 3 m s^{-1} flow rate measured by Weeks (1987) can be duplicated, and if so, what system radius would be required. The pressure gradient applied across the outer two elements is 72 Pa (Weeks, 1987). Determined from a mine climate equation, this is the maximum potential difference between the atmosphere and a borehole.

The first case, Figure 2.8, shows that after about 3 days of simulation time, a flow rate of 3.5×10^{-4} m s^{-1} was calculated, for a radius of 1000 m. This was five orders of magnitude less than the value reported by Weeks (1987). For a 250 m system, velocities increase to 1.9×10^{-3} m s^{-1}. Figure 2.8 shows that as the radius of the system becomes smaller, two things occur. The first is that the equilibration time decreases for the system to reach steady state. Changing the radius from 1000 m to 250 m increases the velocities an order of magnitude. The other characteristic associated with a decreasing system radius is that the pressure gradient becomes steeper toward the well so that velocity increases. Figure 2.9 shows flow rates for a 10 and 5 meter system. For a 5 m system, steady state is reached at about 10^{-4} days (less than 1 minute). The highest flow rate is for a 5 meter system, and is 0.3 m s^{-1}. This is still an order of magnitude less than that measured by Weeks (1987), and at an improbable radius. The topographic model therefore fails to reproduce measured flow rates at Yucca Mountain. This may be so do to lack of information on formation properties, such as permeability, and the complex nature of fractures.

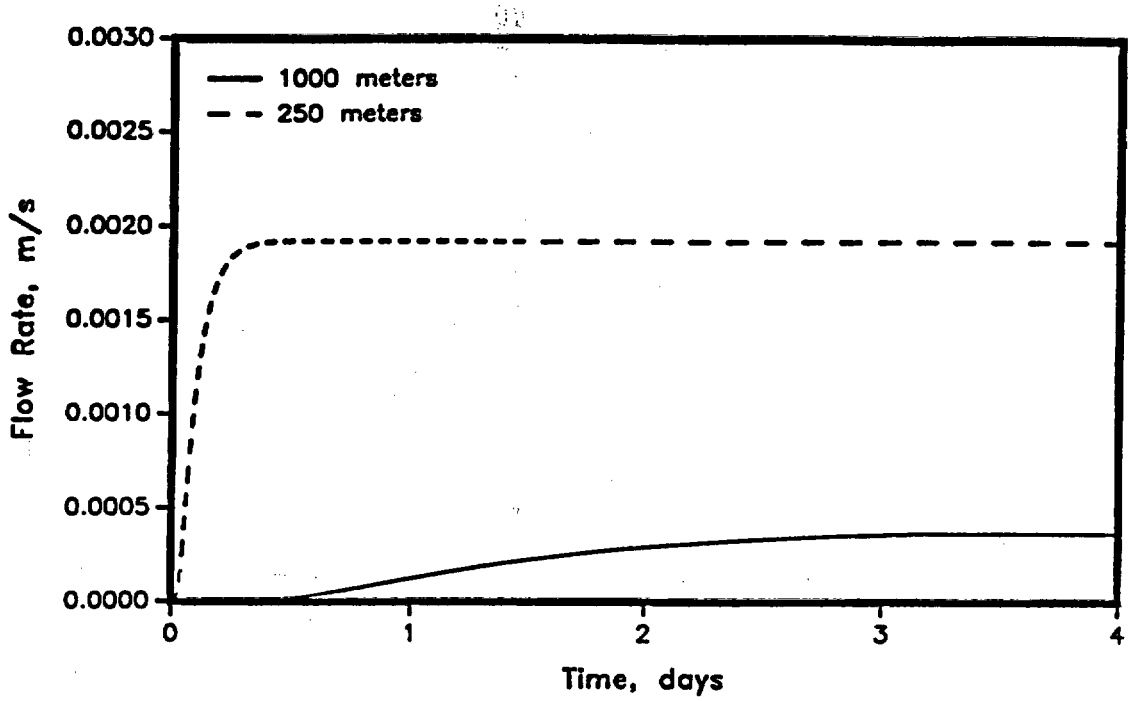

Figure 2.8. Flow rate of air out of borehole vs. time for 72 Pa pressure drop at 1000 m and 250 m, fracture simulations.

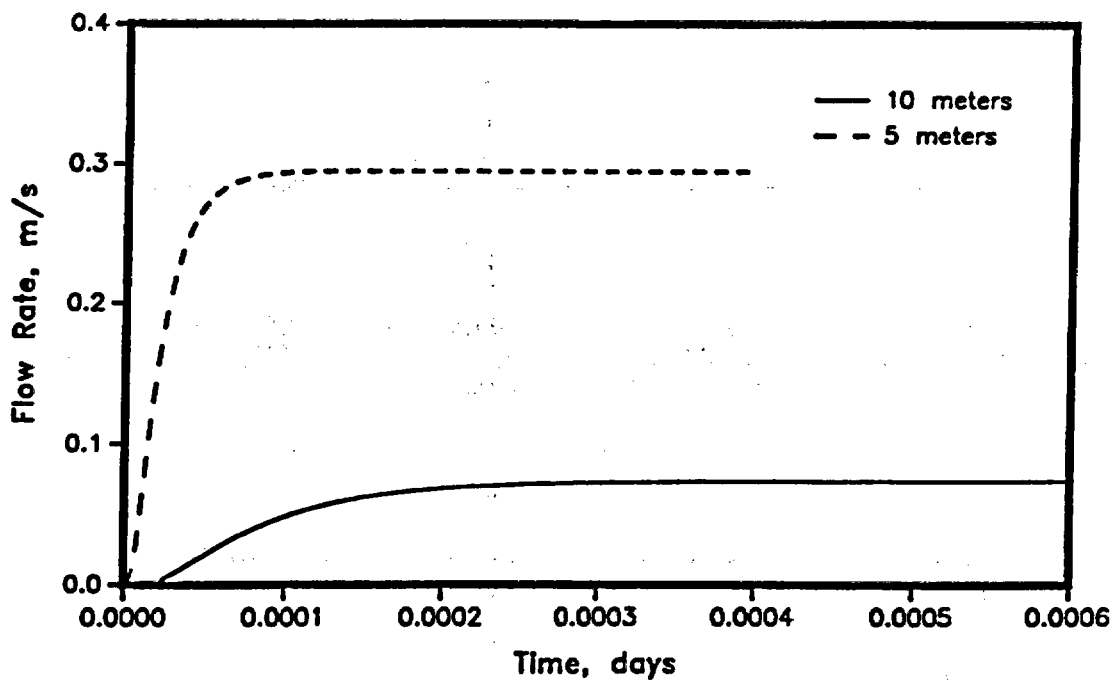

Figure 2.9. Flow rate of air out of borehole vs. time for 72 Pa pressure drop at 10 m and 5 m, fracture simulations.

Chapter 3

MULTIPHASE FLOW SIMULATIONS: THEORY AND DEVELOPMENT

Results from the preliminary single-phase simulations aided in designing the multiphase simulations. The simulations in Chapter 2 did not address the role of water vapor or the interaction between liquid and gas phases. We learned that a typical diurnal barometric pressure disturbance, induced at a borehole, propagates about 1000 m into the surrounding environment, after 2 days. Also, for the conditions specified in the previous chapter, maximum gas flow rates from an open borehole are on the order of 10^{-3} m s^{-1}.

The purpose of this chapter is to develop a more precise model to explore the nature of gas flow through partially saturated rock. The model was formulated around a nonisothermal multiphase, multicomponent computer code. Table 3.1 lists some of the primary differences between the two groups of simulations.

TABLE 3.1. Summary of Differences Between Simulations in Chapter 2 and Chapters 3 and 4.

	Ch. 2 Simulations	Ch. 3,4 Simulations
Flow System Domain	Unsaturated Zone	Tiva Canyon unit
Number of Active Phases	1	2
Number of Components in Gas	1	2
Flow System Dimensions	1	1
Code	GASFLO	TOUGH

The focus of these simulations is gas and liquid movement through the Tiva Canyon unit only. As will be explained further in this chapter, the high fracture

density contributes significantly to gas flow under partially saturated conditions. Figure 3.1 shows the boundaries and boundary conditions of the model.

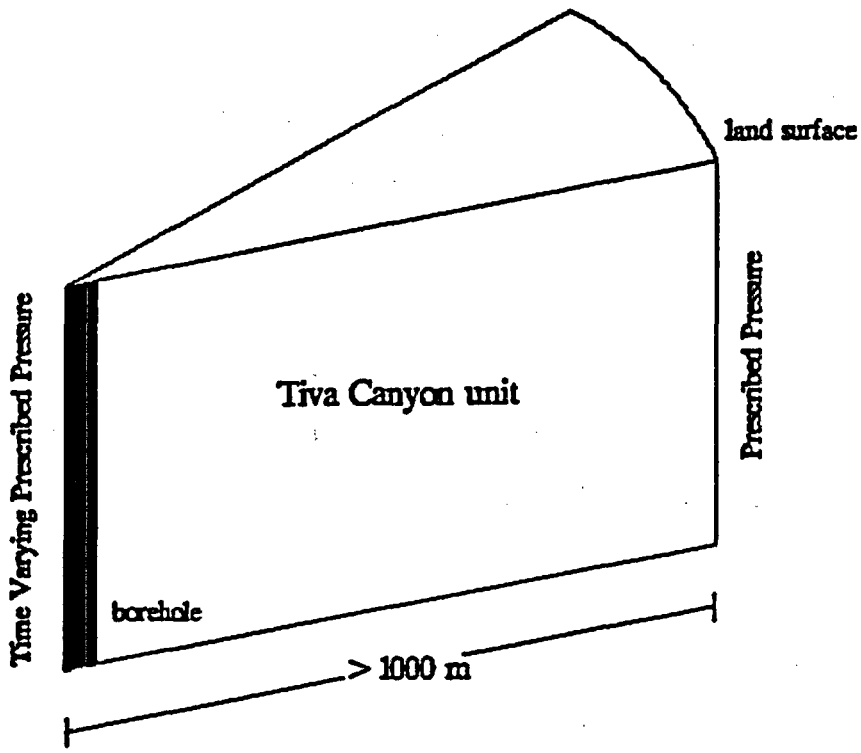

Figure 3.1. Boundaries and boundary conditions for model described in Chapter 3.

These simulations explored several ideas concerning the observed (at Yucca Mountain) and simulated (in the previous chapter) nature of unsaturated gas flow around a borehole. (1) Can a barometrically induced pressure gradient created in an open borehole penetrating unsaturated fractured rock cause enough gas flow in the surrounding formation to be of concern for site characterization? (2) How much water (as vapor) is leaving or entering the system? Is movement controlled by diffusive or convective gas flux? (3) What statements can be made concerning the transient/steady-state nature of this moisture movement?

Governing Equations

The simulator TOUGH (Pruess, 1987) is used to answer the above questions. This code differs from other partial saturation codes primarily because gas is treated as a mobile phase. TOUGH solves a nonlinear mass balance equation for each active phase (liquid, gas) and an energy balance equation for the system. The governing mass and energy balance equations are

$$\frac{d}{dt}\int_{V_n} M^{(\kappa)}\, dV = \int_{\Gamma_n} \mathbf{F}^{(\kappa)} \cdot \mathbf{n}\, d\Gamma + \int_{V_n} q^{(\kappa)}\, dV \tag{3.1}$$

where M denotes accumulation of mass or heat, $\mathbf{F}$ is flux, q is a sink/source, and κ is a component ($\kappa =$ 1: water; $\kappa = 2$: air; $\kappa = 3$: heat).

Mass accumulation is

$$M^{(\kappa)} = n \sum_{\beta=l,g} S_\beta \rho_\beta X_\beta^{(\kappa)} \tag{3.2}$$

where n is porosity, S_β is phase saturation, ρ_β is phase density, $X_\beta^{(\kappa)}$ is mass fraction of component κ within phase β, and β denotes a phase.

Heat accumulation is

$$M^{(3)} = (1-n)\rho_r C_r T + n \sum_{\beta=l,g} S_\beta \rho_\beta u_\beta \tag{3.3}$$

where ρ_r is mass density of the solid, C_r is specific heat of the solid, T is temperature, and u is internal energy of phase β. The first term on the right-hand-side represents heat accumulation in the solid, while the second term represents heat accumulation in the fluids.

Mass flux terms are summed over the two mobile phases:

$$\mathbf{F}^{(\kappa)} = \sum_{\beta=l,g} \mathbf{F}_\beta^{(\kappa)} \tag{3.4}$$

where the flux of each phase is

$$\mathbf{F}_\beta^{(\kappa)} = -k\frac{k_{r\beta}}{\mu_\beta}\rho_\beta X_\beta^{(\kappa)}(\nabla P_\beta - \rho_\beta \mathbf{g}) - \delta_{\beta g} D_{va}\rho_\beta \nabla X_\beta^{(\kappa)} \tag{3.5}$$

Here k is intrinsic permeability, $k_{r\beta}$ is relative permeability of phase β, μ_β is dynamic viscosity of phase β, ∇P_β is the pressure gradient across phase β, g is acceleration due to gravity, and D_{va} is the binary diffusion coefficient for water vapor in air. The kronecker delta, $\delta_{\beta g}$, indicates that binary diffusion is only modeled in the gas phase.

Heat flux is (conduction and convection)

$$\mathbf{F}^{(3)} = -\Lambda\nabla T + \sum_{\substack{\beta=l,g\\ \kappa=1,2}} h_\beta^{(\kappa)}\,\mathbf{F}_\beta^{(\kappa)} \tag{3.6}$$

where Λ is thermal conductivity of the rock-fluid mixture, and $h_\beta^{(\kappa)}$ is the specific enthalpy of component κ in phase β.

Constitutive Relationships

Liquid water retention as a function of pressure head is (van Genuchten, 1980)

$$\theta_l = \theta_r + \frac{(\theta_s - \theta_r)}{[1 + (\alpha\psi)^\beta]^\lambda} \tag{3.7}$$

where θ_l is volumetric moisture content, θ_r is residual moisture content, θ_s is moisture content at saturation, ψ is pressure head, and α, β, and λ are curve fit parameters ($\lambda = 1 - 1/\beta$; $0<\lambda< 1$).

Liquid relative permeability is determined using the water retention function above and the hydraulic conductivity expression of Mualem (1976)

$$k(\theta)_{lr} = \Theta^{1/2}[1 - (1 - \Theta^{1/\lambda})^\lambda]^2 \tag{3.8}$$

where $k(\theta)_{lr}$ is relative permeability as a function of moisture content, and Θ is

the dimensionless moisture content, $\frac{\theta_l - \theta_r}{\theta_s - \theta_r}$. The equation was originally derived by van Genuchten (1980) in terms of relative hydraulic conductivity, though its form as expressed in terms of relative permeability is equivalent.

The binary (vapor-air) diffusion coefficient is determined through the expression (Vargaftik, 1975)

$$D_{va} = \tau n S_g \frac{D_{va}^0}{P} \left(\frac{T + 273.15}{273.15} \right)^{\gamma} \tag{3.9}$$

where τ is a tortuosity factor (dependent upon pore geometry), n is effective porosity, P is pressure, T is temperature, S_g is gas saturation, D_{va}^0 is the air-vapor diffusion coefficient at standard temperature and pressure in a nonporous medium, and γ is a parameter that describes the temperature dependence of diffusion. Flow in this model is nearly isothermal, so γ is zero.

Equivalent Porous Medium

Because the Tiva Canyon unit is fractured, a deterministic equivalent porous medium (EPM) model was developed. This allows fracture and matrix flow to be modeled as a continuum, as opposed to modeling each flow discretely. Unless fractures in a large system have been characterized with respect to size, length, aperture, asperities, and degree of interconnectedness, it is impossible to model fracture flow discretely. This is the case for the Tiva Canyon unit. The EPM model centers around an averaging procedure that incorporates hydraulic properties of both matrix and fractures.

Major assumptions required in developing the EPM follow: (1) Darcy's law is valid for both phases (gas and liquid) in the fractures and matrix; (2) thermodynamic equilibrium exists between the fractures and matrix; and (3) the sum of

the relative permeabilities to gas and water, at any given moisture content is one ($k_{rg} + k_{rl} = 1$). The second assumption implies that matric potential is the same in a fracture as that in the adjacent matrix. This may be justified because flow rates are thought to be slow enough for pressures between matrix and fractures to remain in equilibrium. The third assumption implies that for any given liquid saturation, the two relative permeabilities sum to 1. This assumption is tenuous, as de Marsily (1986, p. 209) states that the sum of the relative permeabilities in multiphase systems is usually variable and is can be either greater or less than 1. Bear (1972, p. 460) lists several possible reasons. In the presence of two fluids where one wets a solid surface (e.g. water wetting grains), theory suggests that the wetting fluid should surround each grain with a thin film, acting to decrease the pore space available for the nonwetting fluid. This means that each fluid may not establish its own flow channel through the medium, as commonly thought. Also, because wettability is hysteretic, relative permeability may depend on a medium's saturation history, as well as the way fluids are distributed in the medium.

Bear (1972) also gives another reason. The two fluids will exert an interference with one another and cause a transfer of viscous forces between each other. This has been termed the "lubrication effect" (Bear, 1972; Montazer, 1982). The upshot is that Darcy's law with permeability dependent only upon saturation may not physically represent the system. The fact that two fluids may transfer viscous forces between each other suggests that the relative permeabilities may be a function of the ratio of the fluid viscosities. Bear (1972, p. 462) concludes by saying that the concept of relative permeability depending only upon saturation is a good approximation for all practical purposes.

The EPM model requires derivation of a relative permeability function that considers flow in both fractures and matrix. This is based upon the assumption

that

$$\bar{k} = k_m + k_f \tag{3.10}$$

which is justified if k_f is determined from an aquifer test in highly fractured rock with low matrix permeability. ($\bar{k}$ is the EPM intrinsic permeability, k_m is matrix permeability, and k_f is fracture permeability.) For example, Thordarson (1983) analyzed aquifer test data from well J-13 (about 4.2 km from UE-25 WT#17) and determined a transmissivity of 120 $m^2\ d^{-1}$ for the Topopah Spring hydrogeologic unit. Because the matrix permeability is so low, Thordarson assumed that the transmissivity value (and its corresponding intrinsic permeability) reflects formation fracture properties. For the Topopah Spring unit, laboratory measurements of matrix hydraulic conductivity are roughly 4 to 5 orders of magnitude less than that determined by Thordarson (Peters et al., 1984). If k_f is determined from laboratory or analytical methods (such as the cubic law), (3.10) will be invalid because hydraulic conductivity derived from the cubic law is determined for each individual fracture, and only for that fracture's width. On the other hand, hydraulic conductivities determined from aquifer tests reflect the properties of the entire formation, taking into account both fractures and matrix.

Relative permeability in fractures and matrix are explicitly defined as

$$k_{rf} = \frac{k(\theta)_f}{k_f} \tag{3.11}$$

$$k_{rm} = \frac{k(\theta)_m}{k_m} \tag{3.12}$$

where k_{rf} is relative permeability in fractures, $k(\theta)_f$ is the effective permeability in the fracture, and k_{rm} and $k(\theta)_m$ are defined similarly for the matrix.

The sum of the unsaturated permeabilities (fractures and matrix) is equal to an unsaturated EPM permeability

$$\bar{k}(\theta) = k(\theta)_f + k(\theta)_m \tag{3.13}$$

where the overstrike indicates that the variable pertains to an EPM. At first, (3.14) may seem incorrect because relative permeability may vary widely with variations in liquid saturation. At complete saturation, flow is dominated by fractures, as discussed above. However, with a slight decrease in saturation, fractures drain, $k(\theta)_f$ becomes zero (to liquid), and liquid flow is controlled by the matrix. The EPM relative permeability is still a sum of the corresponding unsaturated permeabilities, though $k(\theta)_f$ is zero.

Finally, EPM relative permeability is defined similarly to k_r in homogeneous media

$$\bar{k}_r = \frac{\bar{k}(\theta)}{\bar{k}} \tag{3.14}$$

Insertion of (3.10), (3.11), (3.12), and (3.13) into (3.14) gives

$$\bar{k}_r = \frac{k_{rm}\, k_m + k_{rf}\, k_f}{k_m + k_f} \tag{3.15}$$

which describes the EPM relative permeability for a phase (gas, liquid) as a function of corresponding matrix and fracture relative permeabilities and intrinsic permeability of matrix and fractures. This is the expression given in Pruess et al. (1988), though it is underived.

The relative permeability subroutine in TOUGH was modified to include (3.15) as an option. Relative permeabilities in matrix and fractures are first computed separately using the van Genuchten (1980) equation for water retention and Mualem's (1976) expression for relative permeability. EPM relative permeability is then computed using (3.15). A listing of the modified subroutine is in Appendix C.

Input Data

All input data are from published literature. The data are organized into five groups: rock matrix parameters, fracture parameters, thermal parameters, borehole properties, and boundary and initial conditions.

ROCK MATRIX PARAMETERS These data are listed in Table 3.2. The van Genuchten curve-fit parameters, α, λ, and S_{lr} are from Peters et al. (1984, p. 61), who determined the values from drainage of Tiva Canyon cores. The values of k_m and n_m are from Sinnock et al. (1987). Matrix porosity is taken as the median from the range listed in Table 2 in Sinnock et al. (1987).

TABLE 3.2. Model Parameters for Matrix.

k_m [a] m^2	n_m [b]	α [c] Pa^{-1}	λ [d]	S_{lr} [d]
2.55E-18	0.065	8.372E-07	0.3582	0.0020

[a] Calculated from hydraulic conductivity values in Sinnock et al. (1987, p. 7825).
[b] Median porosity from range given in Sinnock et al. (1987, p. 7825).
[c] From Peters et al. (1984, p. 61). Converted from m^{-1} of water to Pa^{-1}.
[d] From Peters et al. (1984, p. 61).

Figure 3.2 is the characteristic curve (ψ vs. S_l) for the Tiva Canyon. It is a representation of ψ vs. S_l for flow through the matrix only. No EPM function for capillary pressure was derived, because ψ is very nearly zero when fractures are wet. This implies that the true characteristic curve (for matrix and fracture flow) only varies from the matrix curve when S_l is nearly saturated (> 0.98). This condition is never present in the model.

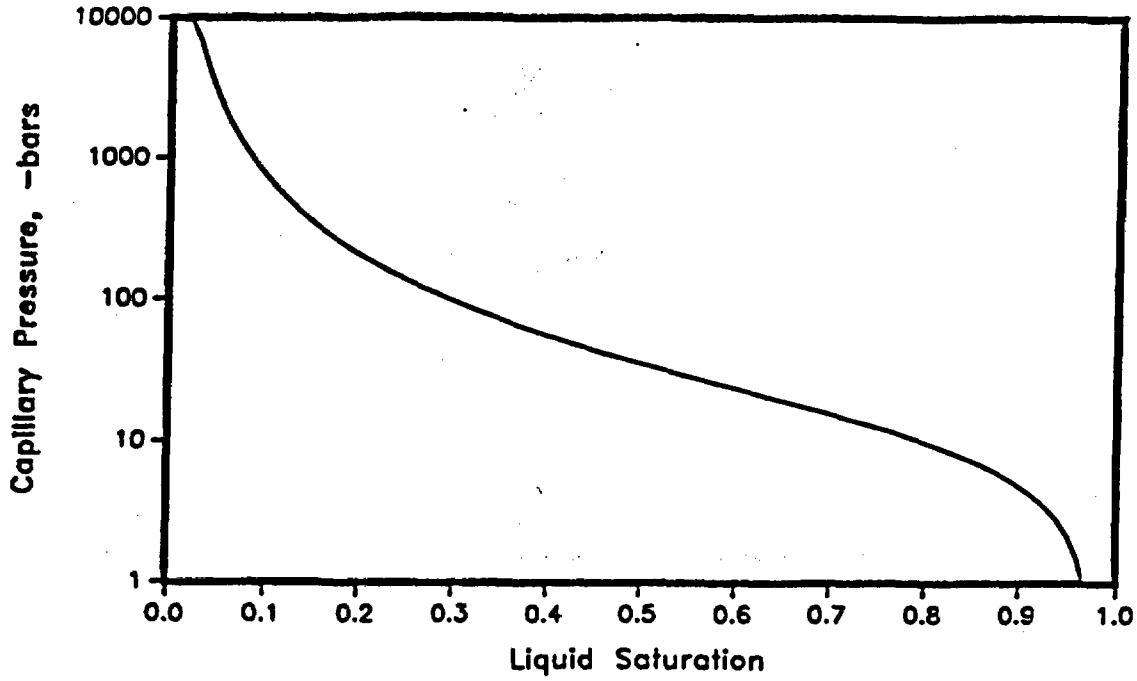

Figure 3.2. Characteristic curve for Tiva Canyon hydrogeologic unit.

FRACTURE PARAMETERS Table 3.3 gives fracture properties for the Tiva Canyon unit. To date, no saturation measurements have been made on fractured cores from Yucca Mountain, though van Genuchten curve fit parameters have been estimated (Klavetter and Peters, 1986). In Table 3.3, n_t is the sum of the matrix (n_m) and fracture (n_f) effective porosities.

TABLE 3.3. Model Parameters for Fractures.

k_f [a] m^2	n_f [b]	n_t [b]	S_{lc} [c]	λ [d]
1.18E-12	0.0018	0.0668	0.973	0.7636

[a] Calculated from hydraulic conductivity values in Sinnock et al. (1987, p. 7825).
[b] From Sinnock et al. (1987, p. 7825).
[c] Calculated using (3.16).
[d] From Klavetter and Peters, (1986, p. 21), $\lambda = 1 - 1/\beta$.

An ad-hoc term "critical saturation" (S_{lc}) is defined as

$$S_{lc} = \frac{n_m}{n_m + n_f} \tag{3.16}$$

where n_m and n_f are the matrix and fracture porosities, respectively. The importance of S_{lc} relates to the EPM model; it is the liquid saturation value at which the fractures become filled. The conceptual model for drainage of a dual porosity medium begins with a saturated (both fractures and matrix) block of rock. Assuming that the average fracture aperture is greater than the average pore diameter, fractures will drain before pores because the pressure head required to drain large voids is greater than (less negative) that required to drain small voids. Peters and Klavetter (1988) measured pressure heads during drainage of fractured rock cores from the Topopah Spring unit and determined that fractures drain at very high matric potential on the order of -1 m. For comparison, in situ matric potential for this unit is estimated as -200 m (Sinnock et al., 1987, p. 7825).

Figures 3.3 and 3.4 are relative permeability as a function of liquid saturation curves (log k_{rl} vs. S_l and log k_{rg} vs. S_l) for the Tiva Canyon unit (S_l is liquid saturation). The Tiva Canyon unit is highly fractured and is modeled as an EPM. Figure 3.3 shows the "double-humped" relationship between k_{rl} and S_l that is characteristic of fractured media. The reason that this characteristic is not seen in Figure 3.3, the log k_{rg} vs. S_l curve, is that the effect is actually present for flow in the fracture, but disguised by the scale of the axes in the figure.

These curves are generated by first computing relative permeability to liquid separately in the matrix and fractures (k_{rm}, k_{rf}), for a given table of liquid saturations. The van Genuchten (1980) expression for pressure head is used with the relative permeability function of Mualem (1976). Equation (3.15) is then used to compute EPM liquid relative permeability. Gas relative permeability is

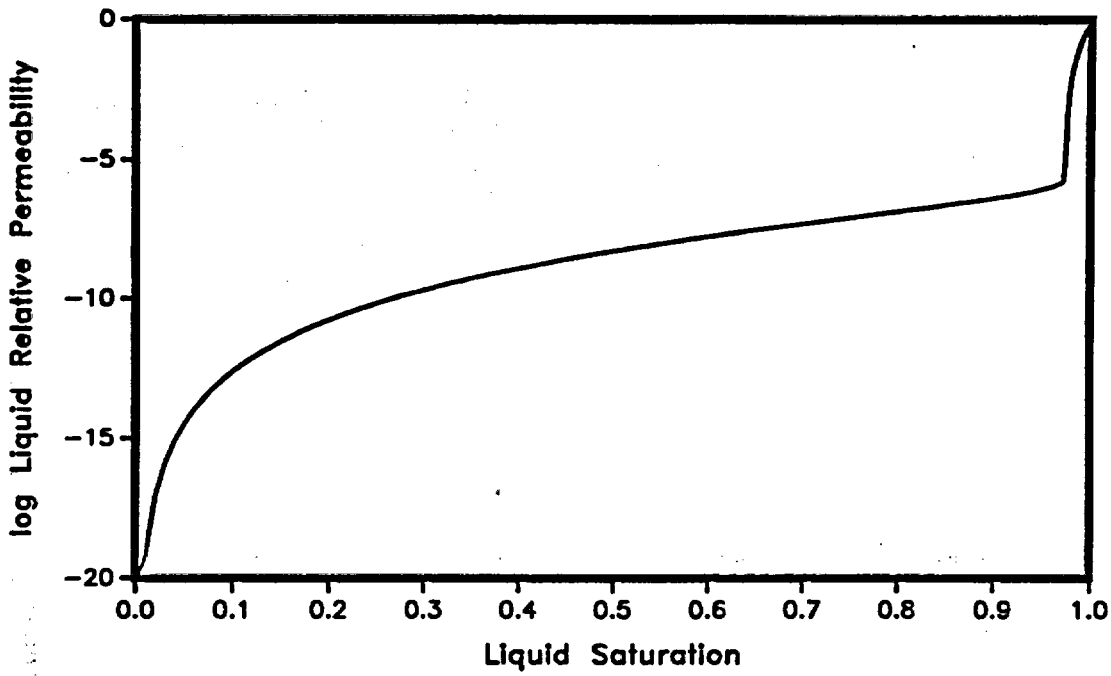

Figure 3.3. Log liquid relative permeability as a function of liquid saturation for Tiva Canyon hydrogeologic unit.

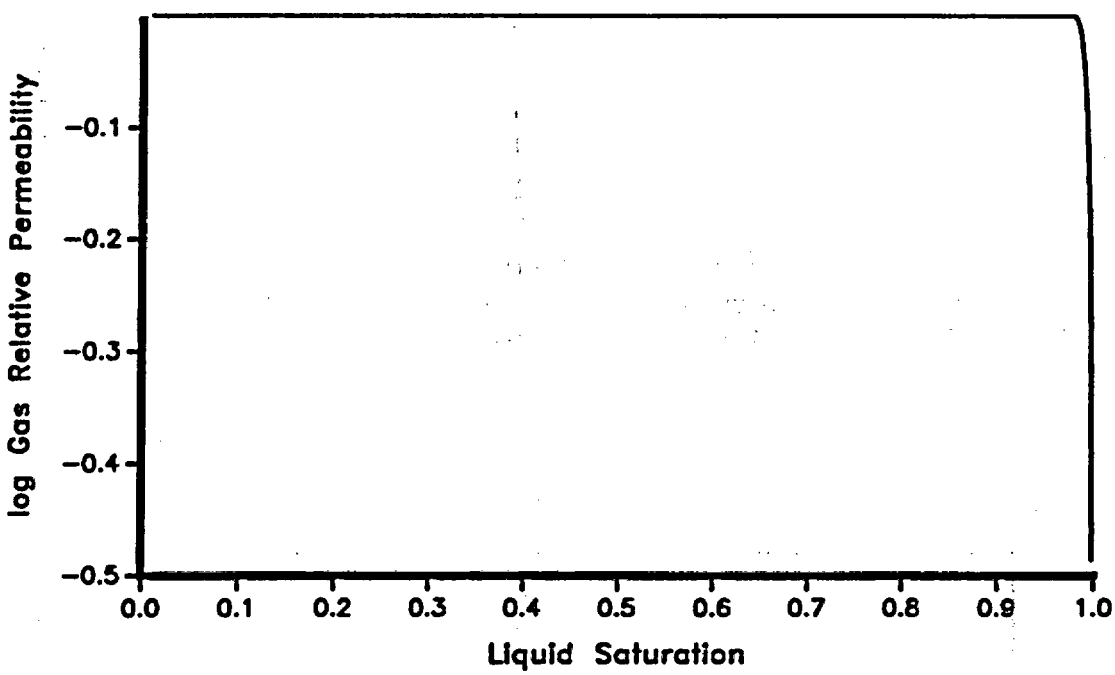

Figure 3.4. Log gas relative permeability as a function of liquid saturation for Tiva Canyon hydrogeologic unit.

$$\bar{k}_{rg} = 1 - \bar{k}_{rl} \tag{3.17}$$

where the subscripts rg and rl refer to EPM relative permeabilities to gas and liquid, respectively.

THERMAL PARAMETERS Because TOUGH solves an energy balance equation, thermal conductivity (Λ) and specific heat (C) are needed as part of the input deck. TOUGH requires formation thermal conductivity under fully saturated conditions; for the Tiva Canyon unit this value is unknown. Sass et al. (1988, p. 26) determined Λ as 1.86 watts $m^{-1}\,K^{-1}$ based on one sample of unsaturated Tiva Canyon. This value is lower than the true saturated value because it contains air, and Λ for air is several orders of magnitude less than water. In spite of this, 1.86 watts $m^{-1}\,K^{-1}$ is assumed as the thermal conductivity of the Tiva Canyon unit under fully saturated conditions.

No experimental data have been obtained for the specific heat of any of the hydrogeologic units at Yucca Mountain (Nimick and Schwartz, 1987). Nimick and Schwartz (1987, p. 56) give estimates of heat capacity per unit mass (specific heat) as a function of temperature for the Topopah Spring unit. These estimates were based on chemical analysis of Topopah Spring tuffs. Because of the physical similarity between the Topopah Spring unit and the Tiva Canyon unit, 770 J $kg^{-1}\,K^{-1}$, estimated at 25°C, is used.

MATERIAL PROPERTIES OF THE BOREHOLE Because the inner vertical boundary of the model is a borehole, it is necessary to define some material properties. Table 3.4 lists the properties to simulate the borehole in the model.

TABLE 3.4. Thermophysical Properties and Their Values Used to Simulate a Borehole.

ρ kg m^{-3}	k m^2	n
2500	1.E-07	0.75

BOUNDARY AND INITIAL CONDITIONS Boundary conditions were determined in the following manner. To simulate a period of high barometric pressure, data was selected from the month of June (Church et al., 1987) when the daily barometric pressure fluctuations are large. June 6, 1984 was chosen and a sine function was fit to the data (Figure 3.5). The function is

$$P(t) = P_0 + A \sin(\frac{2\pi t}{\tau}) \tag{3.18}$$

where $A = 400$ Pa and $\tau = 86{,}400$ sec.

Initial conditions include pressure and gas saturation for each unit. Isothermal flow is assumed. Initial gas saturations are from Sinnock et al. (1987, p. 7825). Table 3.5 lists the initial and boundary conditions for the model.

TABLE 3.5. Initial Conditions Used in the Model.

P [a] Pa	S_g [b]	T °C
87700	0.28	20.0

[a] From Church et al. (1987)
[b] Calculated from liquid saturations in Sinnock et al. (1987, p. 7825).

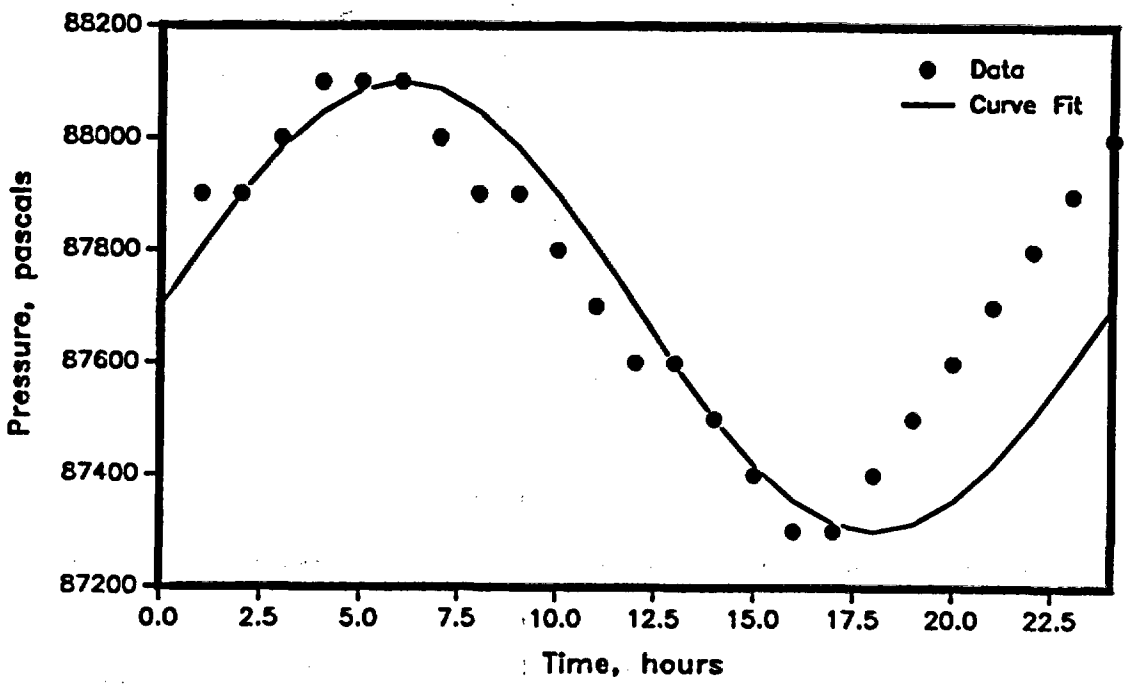

Figure 3.5. Atmospheric pressure data for June 6, 1984 and sine function used as boundary condition for model.

Chapter 4

MULTIPHASE FLOW SIMULATIONS: APPLICATION

The TOUGH code was applied to several types of problems with the intent of identifying the physical phenomena associated with a multiphase flow field around a borehole in the unsaturated zone. Barometric pressure is simulated in the model as a sine wave at the borehole that fluctuates around the initial formation pressure. Therefore the pressure at the borehole is periodically greater than and less than the pressure in the adjacent formation. In order to understand the effects created by this type of fluctuating boundary condition, it is important to separate the components of the wave that are greater than and those that are less than the formation pressure. Step function models were run where (1) the boundary condition at the borehole was greater than the formation pressure (outward-directed pressure gradient), and (2) the boundary condition at the borehole was less than the formation pressure (inward-directed pressure gradient). Given these results, the sine wave model was run and interpreted.

The flow system, governing equations, and constitutive relationships are described in Chapter 3. Radial gas and liquid flow were modeled in a one-dimensional system with a 10 cm radius borehole in the center. Relative humidity in the borehole is zero. Formation properties are those of the Tiva Canyon hydrogeologic unit. Both advective and diffusive (air and water vapor) gas flow were modeled to determine the importance of gas diffusion.

The grid is formulated with 129 elements. Element spacing nearest the borehole is 1 mm; the mesh extends out to 10,000 m. The fine mesh around the well is needed to determine the effects of capillarity, liquid saturation, and temperature around the borehole. A simulation was run with $\bar{k}$ several orders of

magnitude larger than the normal case; for this a coarser mesh was needed in order for the Courant number condition to be satisfied.

Outward-Directed Pressure Gradient

To analyze the effects of an outward pressure gradient, an 88,100 Pa pressure was applied at the borehole at time zero, 400 Pa greater than the initial formation pressure (Figure 4.1). This injects dry air into the humid formation. (Relative

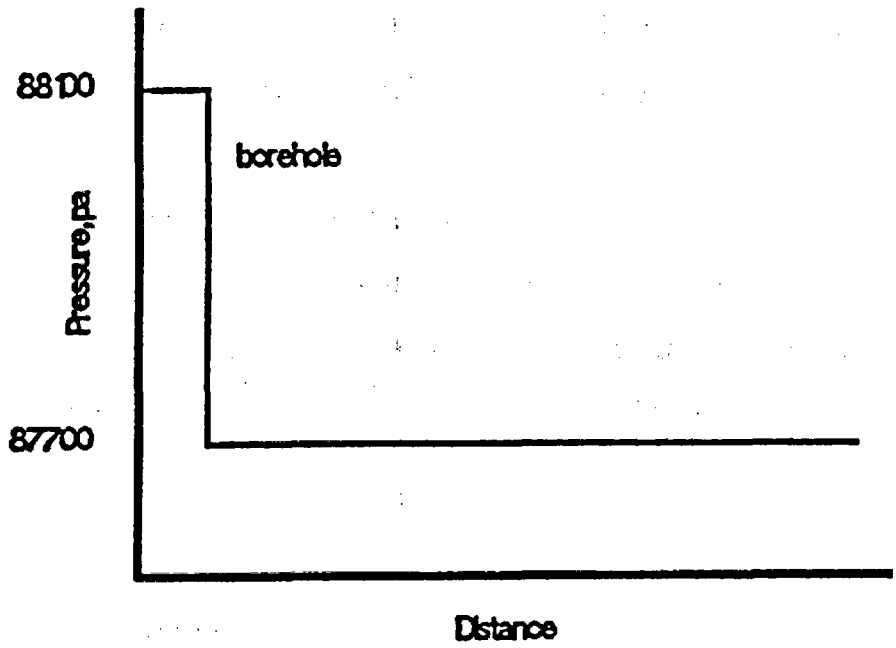

Figure 4.1. Step change pressure condition for outward-directed pressure simulations.

humidity in the Tiva Canyon unit is 0.989 under ambient conditions.) Figure 4.2 shows several effects that occur adjacent to the borehole when this pressure gradient is applied. After 10 hours, dry air blowing into the formation has lowered S_l about 2%, through evaporation of liquid. The initial S_l condition, 0.72, is

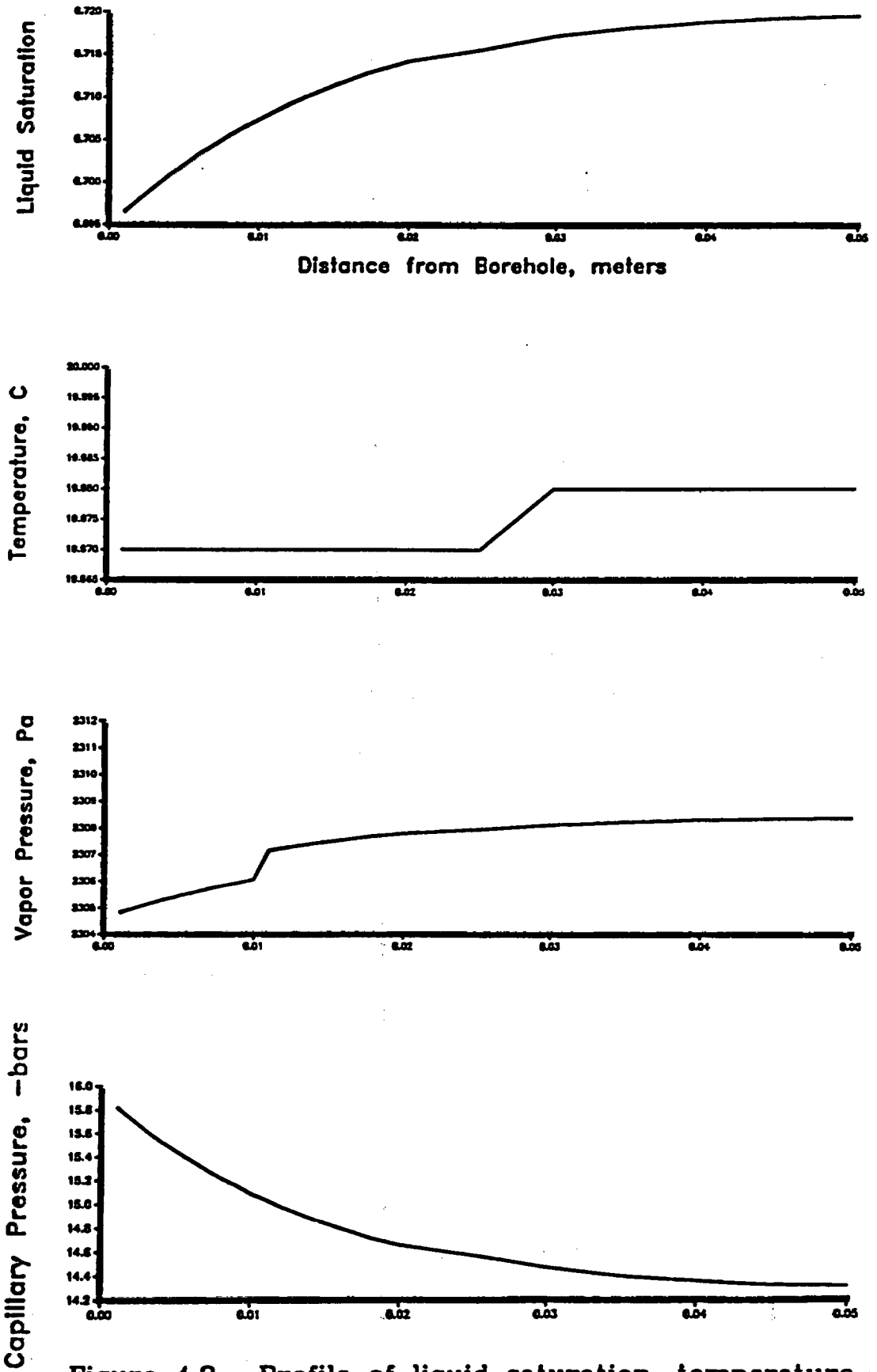

Figure 4.2. Profile of liquid saturation, temperature, vapor pressure, and capillary pressure after 10 hours. Intrinsic permeability is 1.18 x 10^{-12} m^2.

unaffected past 5 cm. In response to evaporation, temperature at the borehole drops about 0.03°C because heat is given off during evaporation. TOUGH computes saturated vapor pressure at each element; vapor pressure (P_v) can then be calculated from a rearrangement of (Hillel, 1980)

$$\psi = \frac{RT}{M} \ln(\frac{P_v}{P_{sat}}) \tag{4.1}$$

where ψ is capillary pressure (joules kg^{-1}), R is the universal gas constant (8.314 J mol^{-1} K), T is temperature (K), M is the molecular weight of water (0.01802 kg mol^{-1}), P_v is the vapor pressure (Pa), and P_{sat} is saturated vapor pressure (Pa). Vapor pressure is lowest where evaporation is highest. This is because both ψ and P_{sat} control P_v; where evaporation is high, ψ is small (more negative) because of drying, and P_{sat} is small because temperature is low. Though the vapor pressure gradient is toward the borehole, both water vapor and air flow away from the borehole in response to the larger air pressure gradient (away from the borehole). The air pressure gradient across the x-axis in Figure 4.2 is 200 Pa m^{-1} while the vapor pressure gradient is 60 Pa m^{-1}.

The drying front establishes a matric potential gradient toward the borehole (Figure 4.2), causing liquid water to flow toward the borehole. Multiphase countercurrent flow develops: gas flow is away from the borehole (into the formation) and liquid flow is toward the borehole. Water (as either vapor or liquid) never leaves the formation because the air pressure gradient forces vapor farther into the formation, and any liquid water that reaches the borehole evaporates, flows back into the formation as vapor, and condenses. Figure 4.3 shows the gas and liquid flow rates within 0.5 m of the borehole. The mass flow rate of gas, 1.741 x 10^{-3} kg sec^{-1}, is constant throughout the domain in Figure 4.3. Mass flow for a phase is defined as ρQ, where ρ is the mass density of the phase and Q is its

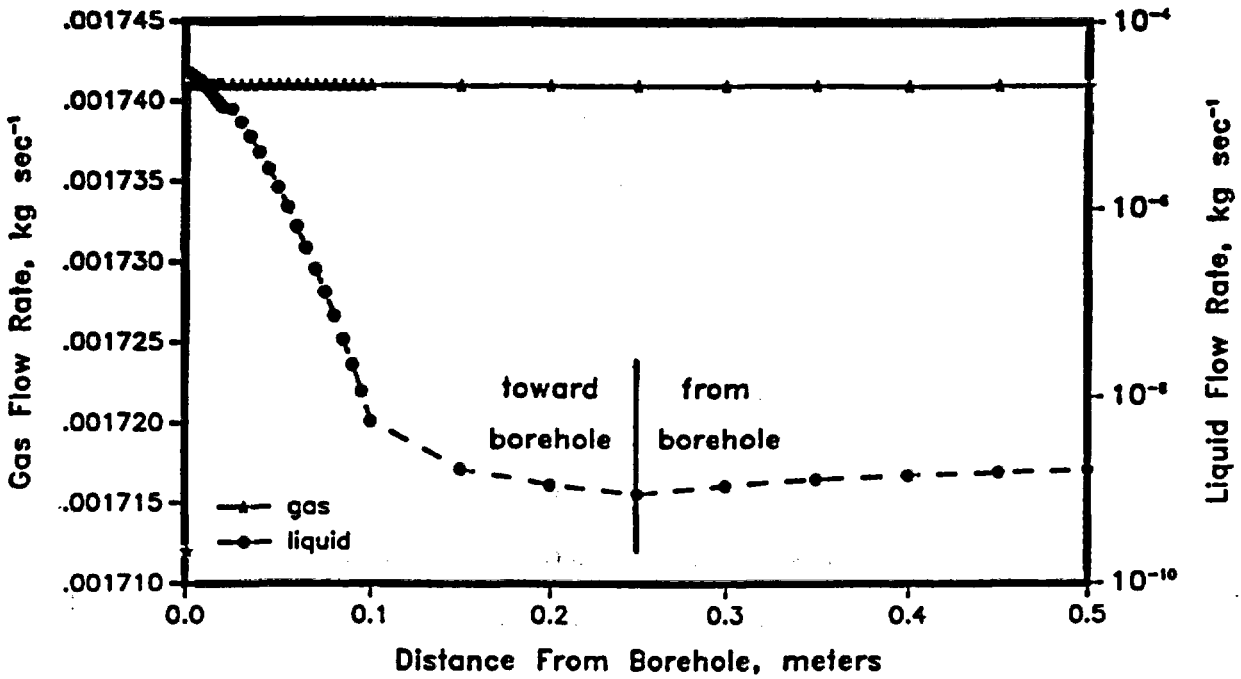

Figure 4.3. Gas and liquid flow rates as a function of distance through the Tiva Canyon unit. Intrinsic permeability is 1.18 x 10^{-12} m^2.

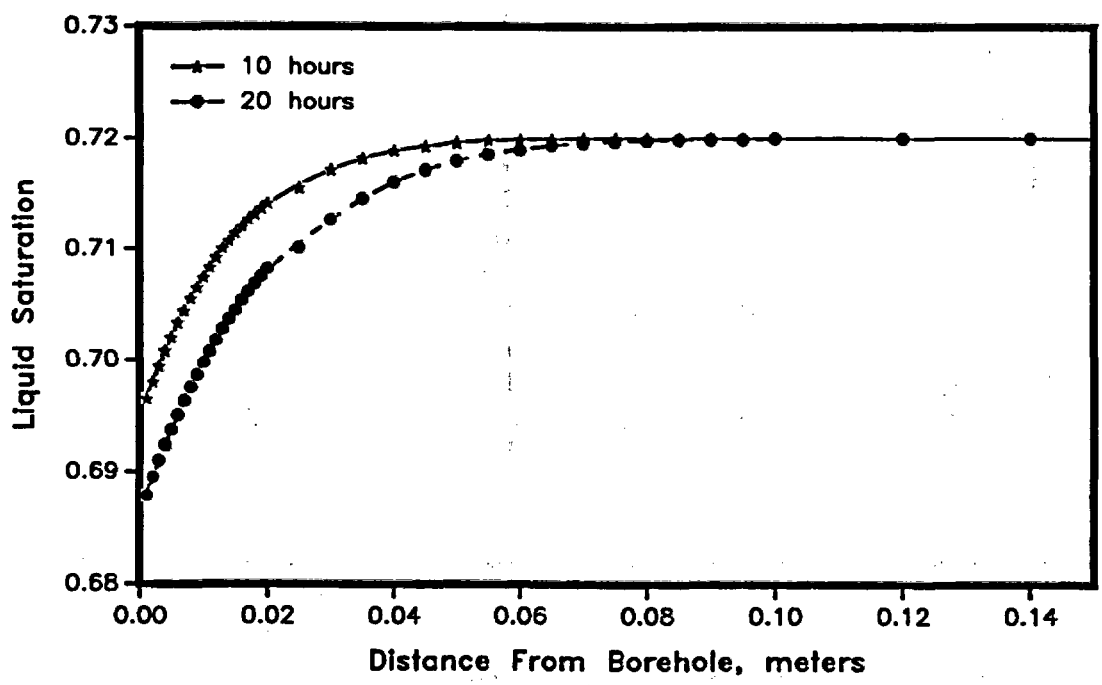

Figure 4.4. Profile of liquid saturation as a function of distance at 10 and 20 hours simulation time.

volumetric discharge. Within several centimeters of the well, air pressure is nearly constant so that a very small gradient exists, which results in little significant compression of the gas. Hence its density remains essentially constant. Q remains constant because when flow is incompressible (which this approximates), volumetric discharge is conserved. Because both Q and ρ are constant within 0.5 m of the borehole, the mass flow rate is constant.

Within 0.25 m of the borehole, liquid flow is the result of a strong matric potential gradient toward the borehole. Past 0.25 m, S_l is constant and the capillary pressure gradient is nonexistent. Figure 4.3 shows that here liquid water moves away from the borehole, though at an insignificant flow rate (10^{-9} kg s^{-1}).

Little change occurs after 10 hours. Figure 4.4 shows S_l as a function of distance for 10 and 20 hours. As anticipated, drying occurs through time, but the effect occurs only about 10 cm from the borehole.

Simulations were performed in which $\bar{k}$ was raised 5 orders of magnitude to 1.18×10^{-7} m^2. (This is equivalent to a gravel; Freeze and Cherry, 1979.) Figure 4.5 presents some results of this simulation. The drying front is more pronounced, the temperature drops from the initial condition, 20°C, to 5°C within 2 m of the borehole, and a steep capillary pressure gradient develops toward the borehole. The saturation gradient extends about 10 m into the formation. The same phenomena described for the medium $\bar{k}$ (1.18×10^{-12} m^2) simulation is seen for the high $\bar{k}$ scenario, though the results are more pronounced.

The above simulations do not include gas diffusion; experiments showed this process to be unimportant. For coupled advection/gas diffusion, equation (3.9) is included in the mass balance equation. The tortuosity factor, τ was chosen as 0.5, and the temperature dependence coefficient, γ was chosen as 1.8 (Vargaftik, 1975). The binary air-vapor diffusion coefficient, D_{va}, was determined from equation

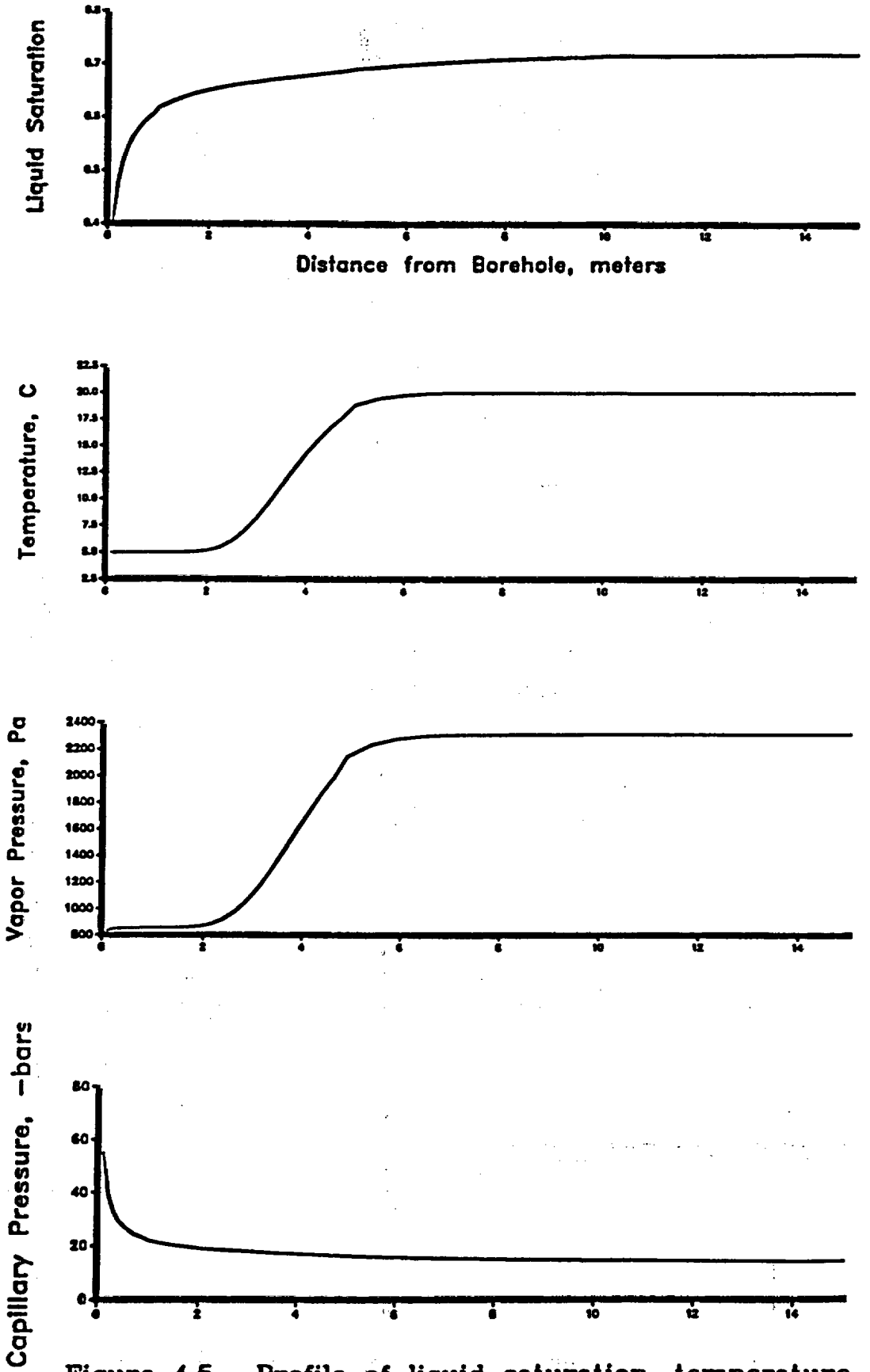

Figure 4.5. Profile of liquid saturation, temperature, vapor pressure, and capillary pressure after 10 hours. Intrinsic permeability is 1.18 x 10^{-7} m^2.

(16.3-1) in Bird et al., (1960, p. 505). D_{va} is 2.87 x 10^{-5} m^2 s^{-1}. Results show that for a 30 hr simulation, capillary pressure, liquid saturation, temperature, and pressure distribution through the formation is identical whether diffusion is turned on or off. This is because the equivalent porous medium permeability, 1.18 x 10^{-12} m^2, is high enough that advective gas flow dominates as the principle transport mechanism.

Inward-Directed Pressure Gradient

To investigate the effects of an inward-directed pressure gradient, simulations were run in which a prescribed pressure of 87,300 Pa was applied at the borehole. This is 400 Pa less than the initial formation pressure (Figure 4.6). Results show that vapor of similar humidity as that of the formation enters the borehole. The pressure wave travels through the formation without any change in initial liquid saturation, capillary pressure, or temperature in any elements. This is due to the

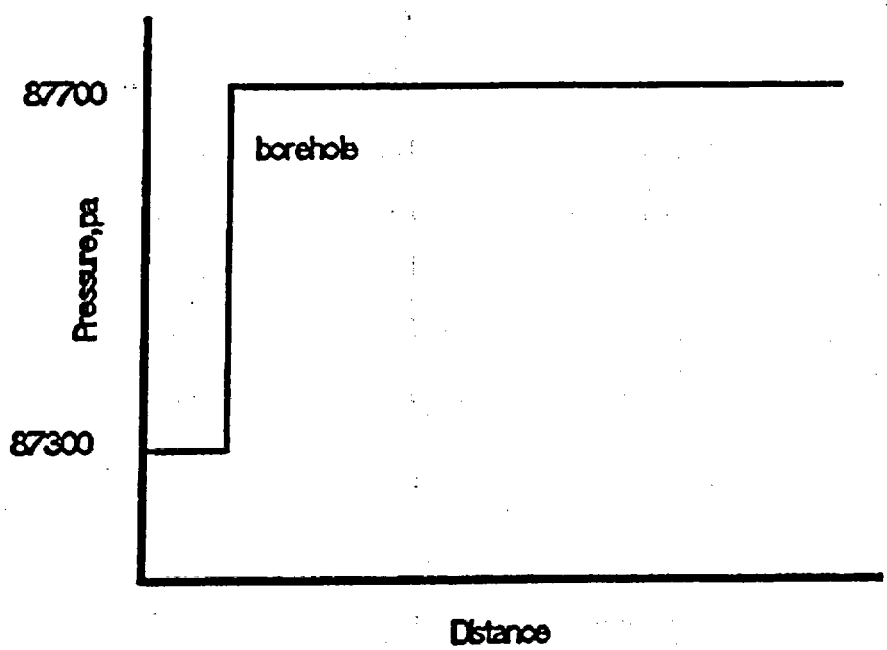

Figure 4.6. Step change pressure condition for inward-directed pressure simulations.

nature of the outer boundary condition. At the outer edge of the system, the boundary condition is prescribed pressure (as opposed to zero flux). This causes the outer boundary to act as an infinite reservoir that maintains its initial conditions. This boundary continuously provides fluid (gas and liquid) into the system, replenishing fluid as it is lost to the borehole. The result is that mass (both gas and liquid) flows toward the borehole, without any change in initial conditions through the formation.

Sinusoidal Pressure Boundary Condition

To analyze the effects of periodically changing conditions, a time-varying sinusoidal pressure wave was prescribed at the borehole (equation 3.18). Results of this simulation determine the time at which steady state is reached and the distance through the formation that the wave travels. Figure 4.7 shows the pressure history at a point 50 m from the borehole. Steady state is defined when the wave dimensions begin to repeat. The first repeating wave ends at about 3.2 days, so steady state is established at this time.

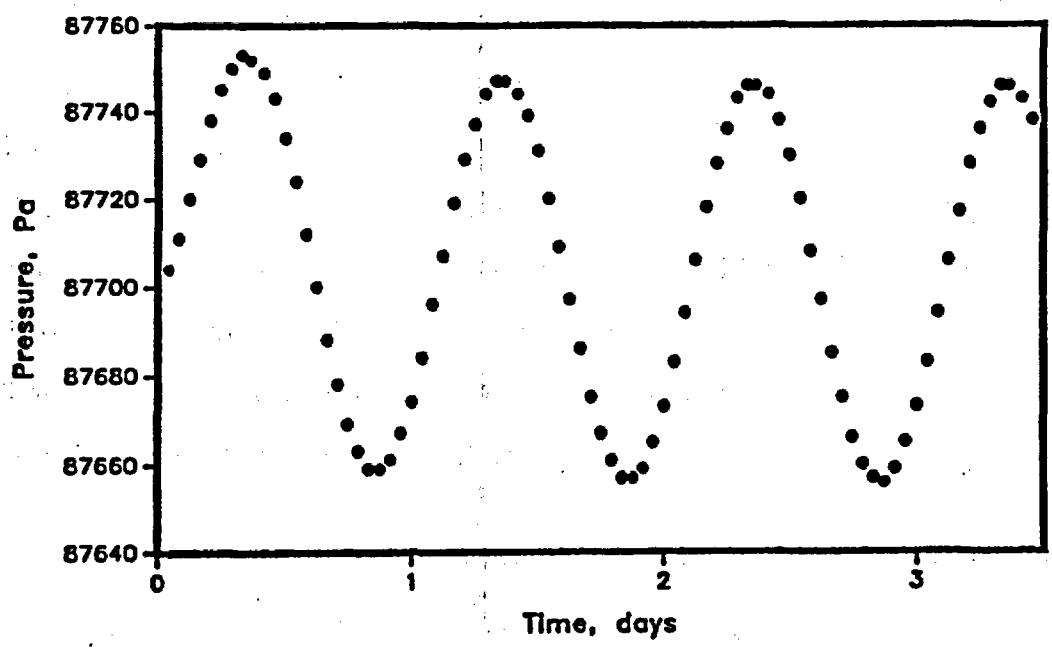

Figure 4.7. Pressure history through Tiva Canyon 50 meters from borehole. Boundary condition at the borehole is equation 3.18

Several steady-state pressure profiles are shown in Figure 4.8. Because the pressure distribution varies regularly, both maximum and minimum values are plotted. The maximum and minimum curves correspond to the profiles at 3.25 and 3.75 days, respectively. The figure shows that at about 160 m (the radius of influence), the formation pressure remains at its initial condition and is unaffected by the borehole disturbance. Close examination of Figure 4.8 reveals that between 40 and 80 m, a slight wave is present in the formation, for a "snapshot" in time. Results from the simulation show that the pressure distribution propagates 40 m through the formation after only 1 hour. This is significant because in the near-field (<40 m), pressure distribution is a strong function of the present borehole boundary condition. The updated borehole pressure has an immediate effect on the pressure in this region because it is superimposed on the existing pressure after a short time. Farther away, remnant pressures are not as affected by the present boundary condition because the propagating wave takes longer to travel and because it has undergone more decay.

Figure 4.9 shows the range of liquid saturations around the borehole. At steady state, within 0.05 m, S_l fluctuates between 0.68 and 0.71. Past 0.05 m, S_l is constant in time, though a spatial gradient exists. The gradient ceases at 0.15 m where the S_l initial condition is unchanged. The countercurrent flow phenomena discussed above occurs with the sinusoidal boundary problem, fluctuating within about 0.5 m of the borehole.

The gas velocities from the borehole are shown in Figure 4.10. At steady state, the velocities range between ± 3 m s^{-1}. The equivalent mass flow rate is 9.8 x 10^{-3} kg s^{-1}. (Gas density varies only 1% in the flow system.) These values were determined by taking the gas phase velocities across the two innermost elements, and substituting them into equation (2.20). The results show that the

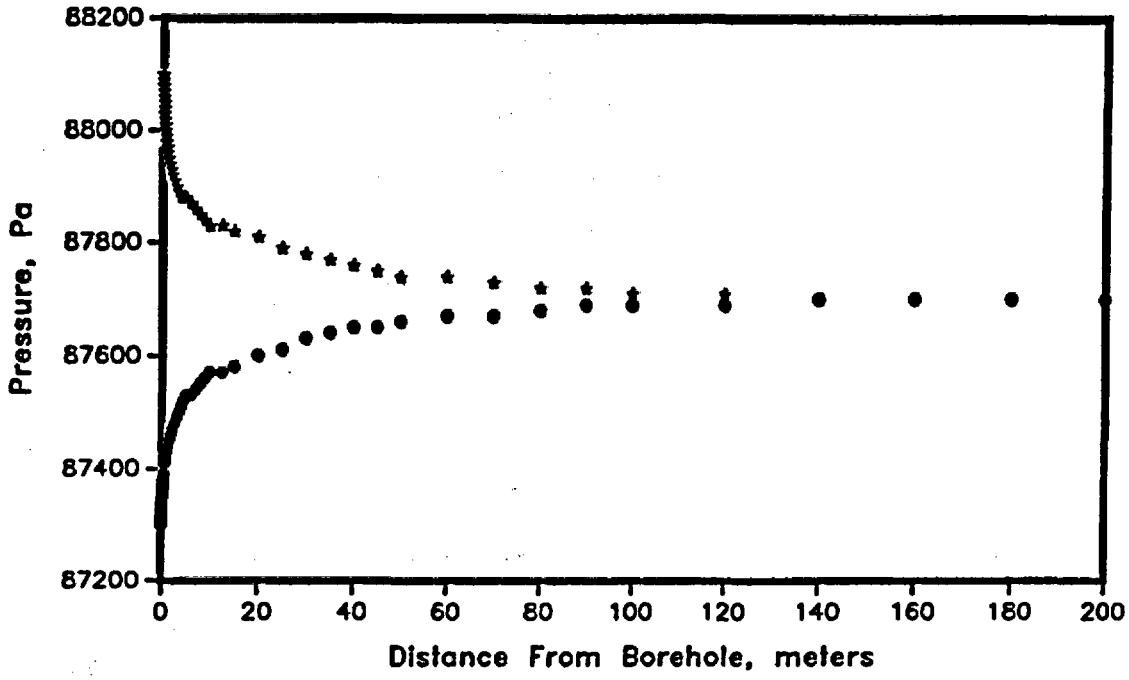

Figure 4.8. Profile of pressure range at steady state for sine wave flow simulation.

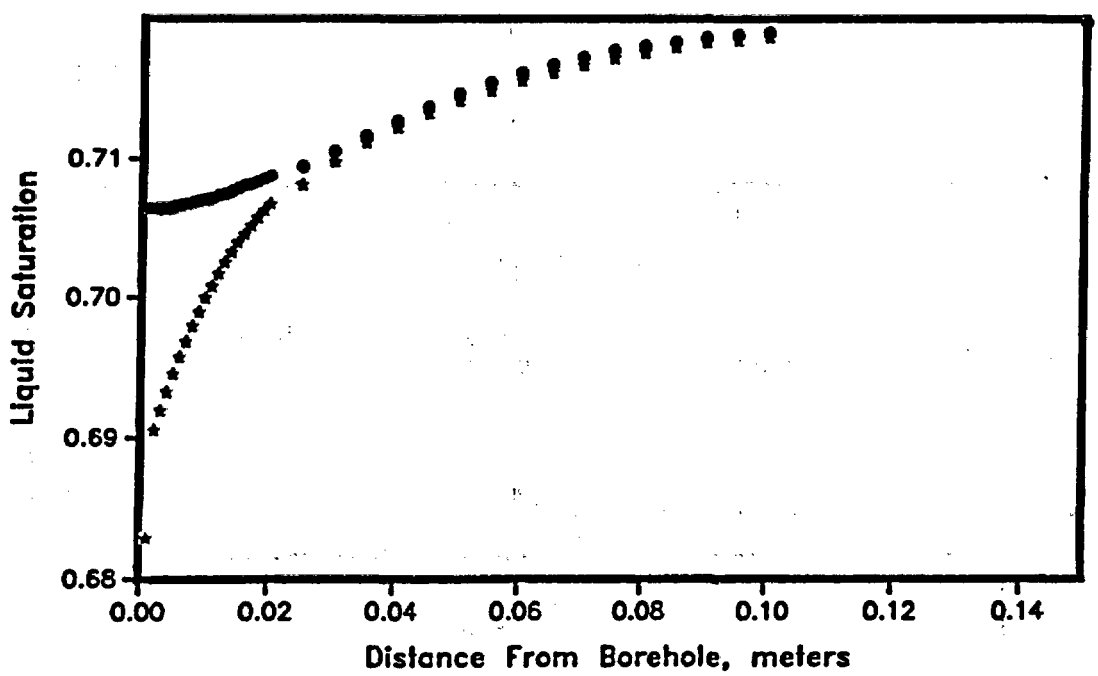

Figure 4.9. Profile of liquid saturation range at steady state for simulation with sine wave pressure condition.

velocities simulated are on the order of those measured by Weeks (1987). The importance is that observed gas phase velocities from a borehole are able to be simulated numerically with a barometric model.

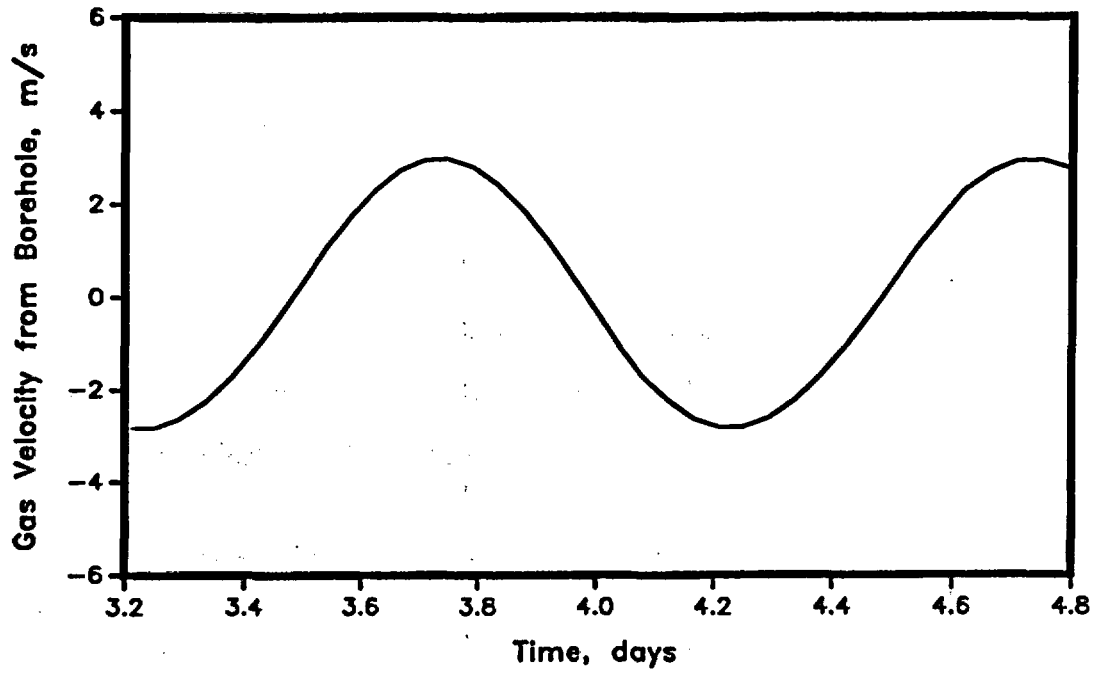

Figure 4.10. Gas velocity from borehole as a function of time for sine wave boundary condition. System is at steady state.

The amount of water vapor leaving the system under steady-state conditions is computed as follows. Over the period of the third day, the mass flow rate of gas ($\hat{q} \equiv \mathrm{M\,t^{-1}}$) entering the borehole was multiplied by X_g^{vap} (mass fraction of vapor in the gas phase, $\frac{\rho_{vap}}{\rho_{gas}}$, for each time step. This gives the mass flow rate of the vapor species in the gas

$$\hat{q}_g^{vap} = \hat{q}_g \, X_g^{vap} \tag{4.2}$$

The equivalent mass of water vapor is determined through

$$m_g^{vap} = \hat{q}_g^{vap} \Delta t \tag{4.3}$$

and the equivalent volume of liquid water

$$V_{w,l} = \frac{m_g^{vap}}{\rho_l} \tag{4.4}$$

where $V_{w,l}$ is the volume of liquid water, m_g^{vap} is the mass of water vapor, Δt is the length of the time step, and ρ_l is the mass density of liquid water. Table 4.2. shows the results of the calculations.

TABLE 4.1. Determination of Equivalent Volume of Water Leaving System During 1 Day.

Time Step	X_g^{vap}	$\hat{q}_g$ kg s^{-1}	$\hat{q}_g^{vap}$ kg s^{-1}	m_g^{vap} kg
84	0.0168	2.161E-4	3.631E-6	1.307E-2
85	0.0168	7.070E-4	1.188E-5	4.276E-2
86	0.0168	1.150E-3	1.932E-5	6.955E-2
87	0.0168	1.514E-3	2.543E-5	9.157E-2
88	0.0168	1.775E-3	2.982E-5	1.075E-1
89	0.0168	1.916E-2	3.219E-5	1.159E-1
90	0.0168	1.927E-3	3.237E-5	1.165E-1
91	0.0168	1.807E-3	3.036E-5	1.093E-1
92	0.0168	1.565E-3	2.629E-5	9.465E-2
93	0.0168	1.216E-3	2.043E-5	7.354E-2
94	0.0168	7.848E-4	1.318E-5	4.746E-2
95	0.0168	2.996E-4	5.033E-6	1.812E-2
				$\sum = 0.90$

The total mass of water lost is 0.90 kg, which when divided by mass density of liquid water (998.3 kg m^{-3}) gives 9.0 x 10^{-4} m^3 of water lost from the

formation per day (0.9 liters d^{-1}).

Pressure Response

Pressure wave efficiency is plotted as a function of distance (Figure 4.11). As expected, wave efficiency decreases away from the borehole. Three separate intrinsic permeabilities were simulated to determine the efficiency's sensitivity to permeability. Efficiency is determined through amplitude decay

$$\text{Amplitude Decay} = \frac{\text{Maximum Wave Amplitude}}{\text{Wave Amplitude at Boundary}} \tag{4.5}$$

Results show that for the normal $\bar{k}$ simulation, wave response is detected as far as 160 m from the borehole. For a formation with $\bar{k}$ two orders of magnitude lower, however, the wave is detected at only 10 m. The normal and high $\bar{k}$ simulations show that efficiency decreases asymptotically away from the borehole. For the low $\bar{k}$ simulation, the grid is too coarse to show accurately the pressure distribution within 10 m of the borehole.

Figure 4.12 is a plot of phase lag for the same intrinsic permeabilities. For the normal case, the pressure wave takes 2 hours to reach its maximum amplitude 30 m from the borehole. This is about the same length of time the wave takes to reach 225 m in the high $\bar{k}$ simulation. In the high $\bar{k}$ simulation, the wave is transmitted nearly instantaneously through the formation up to 250 meters. For all three permeabilities, the results show that the lag-distance trend is linear.

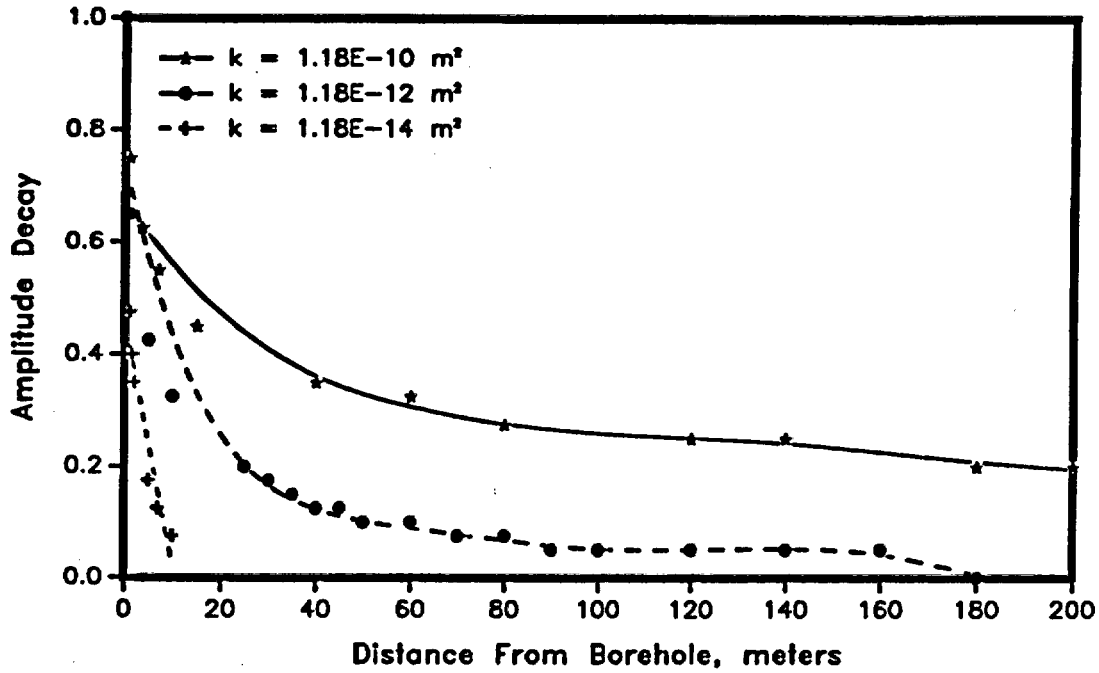

Figure 4.11. Pressure wave efficiency as a function of distance from borehole for three different intrinsic permeabilities.

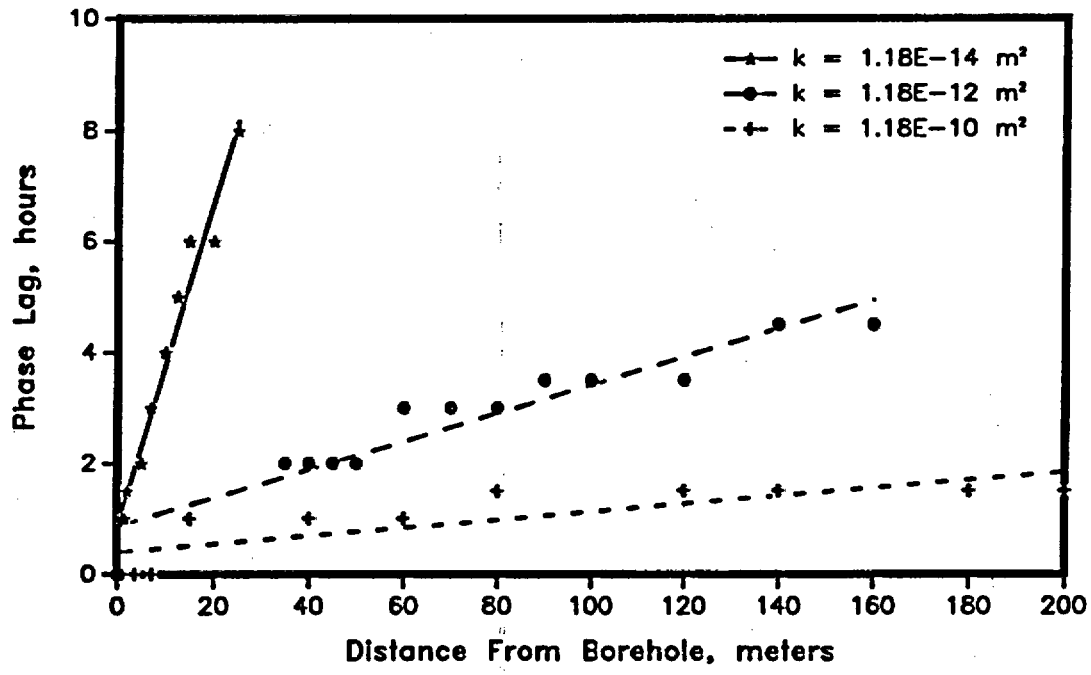

Figure 4.12. Phase lag of pressure wave for three different permeabilities.

Chapter 5

SUMMARY AND CONCLUSIONS

The GASFLO program was useful in testing simple models of air flow through the unsaturated zone. The results provided useful input to guide the more complex, multiphase simulations. Because borehole velocity measurements have not been made for any wells on the east slope of the mountain, the model could not be calibrated. Weeks' (1987) measured velocity of 3.0 m s^{-1} from USW UZ-6 along the ridge of Yucca Mountain is not possible to duplicate, though this value is partly the result of an entirely different driving mechanism. The highest borehole rates are simulated from the fracture model ($\pm$0.0036 m s^{-1}). The models verified that matrix gas flow is negligible compared to fracture gas flow.

The TOUGH code was used to simulate one-dimensional, multiphase, multicomponent, radial flow through the Tiva Canyon hydrogeologic unit. Determined from the EPM model, $\bar{k}$ is 1.18 x 10^{-12} m^2, which is equivalent to a medium sand.

When the borehole pressure is greater than the formation pressure, dry air from the borehole blows into the humid formation. In response to the drop in humidity, liquid water evaporates and S_l drops several per cent. Since heat is given off during evaporation, the temperature around the borehole drops, though an insignificant amount (0.03°C). The air pressure gradient forces gas into the formation, while the lowered S_l around the borehole causes ψ to drop (become more negative) so that liquid water flows toward the borehole. This effect is called multiphase countercurrent flow. However, the entire phenomenon occurs only within 0.25 m of the borehole. Beyond 0.25 m, liquid water flows away from the borehole, in the same direction as the gas phase.

When the borehole pressure is less than the formation pressure, causing gas to blow from the formation, water vapor is lost to the borehole. The physical properties of the formation remain the same because water vapor from farther areas of the system replaces vapor lost to the borehole. This is partly due to the nature of the outer boundary; it is a prescribed pressure boundary that acts as a source for water vapor. This vapor is the same humidity as that escaping to the borehole, hence S_l, ψ, and T remain constant in the formation.

The above simulations helped to understand flow modeled around an uncased borehole with time-varying pressure prescribed at the borehole. Results show that during a typical June day, the pressure wave propagates about 160 m into the surrounding formation. A steady-state wave is established after about 3.2 days. Because of the rather high $\bar{k}$, the wave is transmitted fairly instantaneously over much of the domain. After 1 hour, the pressure wave has traveled 40 m, about one-third the distance it travels at steady state. This is significant because in the near-field (<40 m), the pressure distribution is strongly a function of the present borehole boundary condition. This is emphasized in Figure 4.12; the phase lag is only 2 hours at 40 m. Between 40 and 80 m, a wave exists in the formation, though its amplitude is only about 10 Pa. Past 80 m, the pressure response is so small that a wave, if present, is not discernible.

Liquid saturation varies between 0.68 and 0.71 during this process. Because the formation around the borehole is always drier than the initial S_l, liquid water always flows toward the borehole, irrespective of the direction of gas flow. This condition only occurs within about 0.5 m of the borehole.

Gas phase velocities from the borehole range between ± 3 m s^{-1}, which are on the order of observable velocities in the study area. This is important because it suggests that for the conditions simulated, a barometric model can explain the

cause of the blowing wells on the east flank of Yucca Mountain.

The amount of water leaving the system as vapor is 900 cm^3 d^{-1}. This value can be related to net recharge. Assuming annual recharge is 0.5 mm yr^{-1} (1.4 x 10^{-6} m d^{-1}; Montazer and Wilson, 1984), and the system radius is 160 m, the total volume of water recharged is 1.1 m^3 d^{-1}. The amount of water vapor lost per day (9 x 10^{-4} m^3) is about 0.1% of total recharge. Assuming the recharge estimate is correct, a fairly insignificant percentage of recharge is lost as water vapor. This suggests that the barometric effect may be insignificant in causing the mountain to dry out. Several limitations in the model need to highlighted, however. The model was formulated so that the borehole is single-phase; therefore liquid water never leaves the formation. Water that reaches the borehole/formation interface will collect in the element nearest the borehole, and later evaporate and enter the gas phase. Also, the relative humidity in the borehole is 0.0, so that when air is injected into the formation, it is dry. Actual June relative humidity in the study area is probably between 0.20 and 0.30. In reality, this would replace some of the formation vapor lost to the borehole, hence the atmosphere.

This study demonstrates that a barometric model can explain the cause of the blowing wells on the east flank of Yucca Mountain. In addition, atmospheric pressure fluctuations affect formation air pressures out to 160 m around a borehole, and are likely to produce a net loss of water vapor to the atmosphere. With these results in mind, several suggestions for further research can be proposed. Because the unsaturated zone at Yucca Mountain is deep, a (perhaps) significant temperature gradient exists, and a two-dimensional model could be developed that examines the effects of a geothermal gradient on the system. Montazer and Wilson (1984) postulate that natural thermal convection could be

occurring within the mountain. It is not clear how this might affect gas flow and moisture redistribution in the unsaturated zone. Also, the Topopah Spring unit has similar fracture properties as the Tiva Canyon unit, and it should be incorporated into the multiphase model. A fully two-dimensional, multiphase and energy transport model would help to explore these questions more thoroughly.

References

Aronofsky, J. S. and R. Jenkins, 1954, "A simplified analysis of unsteady radial gas flow," *American Institute of Mining and Metallurgical Engineers-- Transactions*, vol. 201, pp. 149-154.

Baehr, A. L., G. E. Hoag, and M. C. Marley, 1989, "Removing volatile contaminants from the unsaturated zone by inducing advective air-phase transport," *Journal of Contaminant Hydrology*, vol. 4, pp. 1-26.

Bear, J., 1972, *Dynamics of Fluids in Porous Media,* 764 pp., Dover Publications, New York.

Bird, R. B., W. E. Stewart, and E. N. Lightfoot, 1960, *Transport Phenomena,* John Wiley and Sons, 780 pp., New York.

Bixler, N. E., 1985, "NORIA--A finite element computer program for analyzing water, vapor, air, and energy transport in porous media," *SAND84-2057,* Sandia National Laboratories, Albuquerque, New Mexico.

Carman, P. C., 1956, *Flow of Gases Through Porous Media,* 182 pp., Academic Press, London.

Church, H. W., D. L. Freeman, K. Boro, and R. T. Egami, 1987, "Meteorological tower data for the Yucca Alluvial (YA) Site and Yucca Ridge (YR) Site, July, 1983 - October, 1984, final data report," *Rpt. SAND86-2533,* 12 pp., Sandia National Laboratories, Albuquerque, New Mexico.

de Marsily, G., 1986, *Quantitative Hydrogeology,* Academic Press, 440 pp., Orlando, Florida.

Evans III, R. B., G. M. Watson, and E. A. Mason, 1961, "Gaseous diffusion in porous media at uniform pressure," *Journal of Chemical Physics,* vol. 35, pp. 2076-2083.

Evans III, R. B., G. M. Watson, and E. A. Mason, 1962, "Gaseous diffusion in porous media, II, Effect of pressure gradients," *Journal of Chemical Physics,* vol. 36, pp. 1894-1902.

Fairbanks, H. W., 1896, "Note on a breathing gas well," *Science,* pp. 693-694.

Freeze, R. A. and J. A. Cherry, 1979, *Groundwater,* 604 pp., Prentice-Hall, Englewood Cliffs, New Jersey.

Hadley, R. G., 1985, "PETROS - A program for calculating transport of heat, water, vapor, and air through a porous material," *Rpt. SAND84-0878,* 67 pp., Sandia National Laboratories, Albuquerque, New Mexico.

Hillel, D., 1980, *Fundamentals of Soil Physics,* 413 pp., Academic Press, Orlando, Florida.

Jacob, C. E., 1940, "On the flow of water in an elastic artesian aquifer," *Transactions, American Geophysical Union*, vol. 21, pp. 574-586.

Kemper, W. D., J. A. Bondurant, J. Cary, and F. W. Kemper, 1986, "Convective transport in the vapor phase in fractured rock," paper presented at Unsaturated Rock/Contaminated Transport, Nuc. Reg. Comm. and Univ. of Arizona, January 6-9, 1986.

Kipp, K. L., 1987, "Effect of topography on gas flow in unsaturated fractured rock--numerical simulation," *Flow and Transport Through Unsaturated Fractured Rock (Geophysical Monograph 42)*, pp. 171-176, American Geophysical Union, Washington, D.C..

Klavetter, E. A. and R. R. Peters, 1986, "Estimation of hydrologic properties of an unsaturated, fractured rock mass," *Rpt. SAND84-2642*, 55 pp., Sandia National Laboratories, Albuquerque, New Mexico.

Knapp, R. B., 1987, "An approximate calculation of advective gas phase transport of carbon-14 at Yucca Mountain, Nevada," *UCRL-preprint 97805*, 26 pp., Lawrence Livermore National Laboratory, Livermore, California.

McWhorter, D. and D. K. Sunada, 1977, *Ground-Water Hydrology and Hydraulics*, 290 pp., Water Resources Publications, Littleton, Colorado.

Milly, P. C. D., 1982, "Moisture and heat transport in hysteretic, inhomogeneous porous media: A matric head-based formulation and a numerical model," *Water Resources Research*, vol. 18, pp. 489-498.

Montazer, P., 1982, "Permeability of unsaturated, fractured metamorphic rocks near an underground opening," Ph.D. dissertation, 617 pp., Colorado School of Mines, Golden Colorado.

Montazer, P. and W. E. Wilson, 1984, "Conceptual hydrologic model of flow in the unsaturated zone, Yucca Mountain, Nevada," *U.S. Geological Survey Water Resources Investigations 84-4345*, 155 pp., Lakewood, Colorado.

Mualem, Y., 1976, "A new model for predicting the hydraulic conductivity of unsaturated porous media," *Water Resources Research*, vol. 12, no. 3, pp. 513-522.

Muller, D. C. and J. E. Kibler, 1985, "Preliminary analysis of geophysical logs from the WT series of drill holes, Yucca Mountain, Nye County, Nevada," *U.S. Geological Survey Open-File Report 86-46*, 30 pp., Denver, Colorado.

Muskat, M., 1937, *Flow of Homogeneous Fluids*, McGraw Hill, 763 pp., New York.

Nimick, F. B. and B. M. Schwartz, 1987, "Bulk, thermal, and mechanical properties of the Topopah Spring Member of the Paintbrush Tuff, Yucca Mountain, Nevada," *Rpt. SAND85-0762*, 180 pp., Sandia National Laboratories , Albuquerque, New Mexico.

Norum, D. I. and J. N. Luthin, 1968, "The effects of entrapped air and barometric fluctuations on the drainage of porous mediums," *Water Resources Research*, vol. 4, pp. 417-424.

Ortiz, T. S., R. L. Williams, F. B. Nimick, B. C. Whittet, and D. L. South, 1985, "A three-dimensional model of reference thermal/mechanical and hydrological stratigraphy at Yucca Mountain, southern Nevada," *Rpt. SAND84-1076*, 76 pp.

Peck, A. J., 1960, "The water table as affected by atmospheric pressure," *Journal of Geophysical Research*, vol. 65, pp. 2383-2388.

Peters, R. R. and E. A. Klavetter, 1988, "A continuum model for water movement in an unsaturated fractured rock mass," *Water Resorces Research*, vol. 24, pp. 416-430.

Peters, R. R., E. A. Klavetter, I. J. Hall, S. C. Blair, P. R. Heller, and G. W. Gee, 1984, "Fracture and matrix hydrologic characteristics of tuffaceous materials from Yucca Mountain, Nye County, Nevada," *Rpt. SAND84-1471*, 64 pp., Sandia National Laboratories, Albuquerque, New Mexico.

Philip, J. R. and D. A. de Vries, 1957, "Moisture movement in porous materials under temperature gradients," *Transactions, American Geophysical Union*, vol. 38, pp. 222-232.

Pruess, K., 1987, "TOUGH User's Guide," *Rpt. LBL-20700*, 78 pp., Lawrence Berkeley Laboratory, Berkeley, California.

Pruess, K., J. S. Y. Wang, and Y. W. Tsang, 1988, "Effective continuum approximation for modeling fluid and heat flow in fractured porous tuff," *Rpt. SAND86-7000*, 99 pp., Sandia National Laboratores, Albuquerque, New Mexico.

Sass, J. H., A. H. Lachenbruch, W. W. Dudley, S. S. Priest, and R. J. Munroe, 1988, "Temperature, thermal conductivity, and heat flow near Yucca Mountain, Nevada: some tectonic and hydrologic implications," *U.S. Geological Survey Open-File Report 87-649*, 118 pp.

Scott, R. B. and M. Castellanos, 1984, "Stratigraphic and structural relations of volcanic rocks in drill holes USW GU-3 and USW G-3, Yucca Mountain, Nye County, Nevada," *U.S. Geological Survey Open-File Report 84-491*, Denver, Colorado.

Scott, R. B., R. W. Spengler, S. Diehl, A. R. Lappin, and M. P. Chornack, 1983, "Geologic character of tuffs in the unsaturated zone at Yucca Mountain, southern Nevada," *Role of the Unsaturated Zone in Radioactive and Hazardous Waste Disposal*, pp. 289-335, Ann Arbor Science Publishers, Ann Arbor, Michigan.

Sinnock, S., Y. T. Lin, and J. P. Brannen, 1987, "Preliminary bounds on the expected postclosure performance of the Yucca Mountain repository site, southern Nevada ," *Journal of Geophysical Research*, vol. 92, no. B8, pp. 7820-

7842.

Sophocleous, M., 1979, "Analysis of water and heat flow in unsaturated-saturated porous media," *Water Resources Research*, vol. 15, pp. 1195-1206.

Spengler, R. W. and M. P. Chornack, 1984, "Stratigraphic and structural characteristics of volcanic rocks in core hole USW G-4, Yucca Mountain, Nye County, Nevada," *U.S. Geological Survey Open-File Report 84-789*, Denver, Colorado.

Spengler, R. W., F. M. Byers, and J. B. Warner, 1981, "Stratigraphy and structure of volcanic rocks in drill hole USW G-1, Yucca Mountain, Nye County, Nevada," *U.S. Geological Survey Open-File Report 81-1349*, Denver, Colorado.

Thordarson, W., 1983, "Geohydrologic data and test results from well J-13, Nevada Test Site, Nye County, Nevada," *U.S. Geological Survey Water Resources Investigations 83-4171*, Denver, Colorado, 57 pp.

Thorstenson, D. C. and D. W. Pollock, 1989, "Gas transport in unsaturated zones: Multicomponent systems and the adequacy of Fick's laws," *Water Resources Research*, vol. 25, pp. 477-507.

Turk, L. J., 1975, "Diurnal fluctuations of water tables induced by atmospheric pressure changes," *Journal of Hydrology*, vol. 26, pp. 1-16.

Updegraff, C. D. and J. B. Bonano, 1988, "Comparison of strongly heat-driven flow codes for unsaturated media," paper presented at the International Conference and Workshop on the Validation of Flow and Transport Models for the Unsaturated Zone, May 22-25, New Mexico State University, Albuquerque.

van Genuchten, M. Th. 1980, "A closed-form equation for predicting the hydraulic conductivity of unsaturated soils," *Soil Science Society of America Journal*, vol. 44, no. 5, pp. 892-898.

Vargaftik, N. B., 1975, *Tables on the Thermophysical Properties of Liquids and Gases, Second Edition,* John Wiley and Sons, New York.

Wang, J. S. Y. and T. N. Narasimhan, 1985, "Hydrologic mechanisms governing fluid flow in a partially saturated, fractured, porous medium," *Water Resources Research*, vol. 21, pp. 1861-1874.

Weeks, E. P., 1979, "Barometric fluctuations in wells tapping deep unconfined aquifers," *Water Resources Research*, vol. 15, pp. 1167-1176.

Weeks, E. P., 1987, "Effect of topography on gas flow in unsaturated fractured rock: concepts and observations," *Flow and Transport Through Unsaturated Fractured Rock (Geophysical Monograph 42)*, pp. 165-170, American Geophysical Union, Washington, D.C.

APPENDIX A

Notation

A	Area, L^2
A	Pressure wave amplitude, $M\ L^{-1}\ t^{-2}$
b	Thickness, L
C	Specific heat, $L^2\ M^{-1}\ t^{-2}\ T^{-1}$
D_{va}	Diffusion coefficient for water vapor in air, $L^2\ t^{-1}$
D_{va}^0	Diffusion coefficient for water vapor in air at STP, $L^2\ t^{-1}$
F	Source and/or sink, $M\ L^{-3}\ t^{-1}$
F	Flux (in the general sense)
g	Acceleration due to gravity, $L\ t^{-2}$
h	Specific enthalpy, $M\ L^2\ t^{-2}$
k	Intrinsic permeability, L^2
$\bar{k}$	Vertically averaged intrinsic permeability; EPM intrinsic permeability, L^2
k_r	Relative permeability, dimensionless
$\bar{k}_r$	EPM relative permeability, dimensionless
m	Mass
M	Accumulation of mass or heat; molecular weight, $M\ mol^{-1}$
n	Porosity, dimensionless
P	Pressure, $M\ L^{-1}\ t^{-2}$
q	Source, equation (3.1); specific discharge, $L\ t^{-1}$
$\hat{q}$	Mass flow, $M\ t^{-1}$
Q	Volumetric discharge of gas, $M^3\ t^{-1}$
r	Radius, L
R	Universal gas constant, $M\ L^2\ t^{-2}\ mol^{-1}\ T^{-1}$
S_l	Liquid saturation, $\frac{V_w}{V_v}$ dimensionless
S_{lc}	"Critical saturation," $\frac{n_m}{n_m + n_f}$, dimensionless
t	Time
T	Temperature
u	Internal energy of fluid, $M\ L^2\ t^{-2}$
U	Pressure squared, dependent variable in GASFLO, $M^2\ L^{-2}\ t^{-4}$
V	Volume, L^3
X	Component mass fraction of a phase, dimensionless

x,y,z Spatial coordinates, L

Greek

α van Genuchten curve fit parameter, $M\ L^{-1}\ t^{-2}$

γ Temperature dependence on diffusion, dimensionless

δ Kronecker delta, dimensionless

η Moles of a substance

θ_l Volumetric moisture content, $\frac{V_w}{V_t}$, dimensionless

θ_g Volumetric gas content, dimensionless

$\overline{\theta}_g$ Vertically averaged volumetric gas content, dimensionless

Θ Dimensionless water content

Γ Boundary of domain, L^2

λ van Genuchten curve fitting parameter, dimensionless

Λ Thermal conductivity, $M\ L\ t^{-3}\ T^{-1}$

μ Dynamic viscosity, $M\ L^{-1}\ t^{-1}$

ρ Mass density, $M\ L^{-3}$

τ Wave period, t; tortuosity, dimensionless

Ω Volume of domain, L^3

Subscripts

a Air

f Fracture

g Gas

j Position (in finite difference equations)

l Liquid

m Matrix

r Residual, as in S_r; relative, as in k_r, rock, as in C_r

s Saturation

sat Saturated

t Total (as in V_t, total volume)

v Voids; vapor (as in P_v, vapor pressure)

w Water

β Phase

Superscripts

κ	Phase component (1=water, 2=air, 3=heat)
n	Time step
vap	Vapor

General

$\bar{\ }$	Overstrike, variable underneath pertains to EPM
bold	Denotes the variable as a vector
TCw	Tiva Canyon welded hydrogeologic unit
TSw	Topopah Spring welded hydrogeologic unit
CHz	Calico Hills zeolitic hydrogeologic unit
PPw	Prow Pass welded hydrogeologic unit

APPENDIX B

```
c     This program solves the one-dimensional equation for
c     single phase gas flow in unsaturated porous media
c     with constant viscosity, permeability, and porosity,
c     in radial coordinates.
c
c     Clay A. Cooper  December, 1988
c
c     a = subdiagonal vector of coefficient matrix
c     b = diagonal vector of coefficient matrix
c     c = superdiagonal vector of coefficient matrix
c     dr = radius of each element [meters]
c     dt = time step size [seconds]
c     epsil = effective porosity [dimensionless]
c     kf = first equation (for tridag routine purposes)
c     l = last equation (for tridag purposes)
c     lbc = left hand boundary condition
c     mu = gas dynamic viscosity [kg /(meter * second)]
c     n = number of nodes
c     imax = number of time steps
c     itran = flag to identify time-varying boundary conditions
c       (use 1 for transient bc's; 2 for constant pressure bc)
c     perm = intrinsic permeability [meters squared]
c     press = pressure [newtons / meter squared]
c     pressi = initial pressure [newtons / meter squared]
c     r = right hand vector
c     rbc = right hand boundary condition
c     t = time [seconds]
c     thick = formation thickness [meters]
c     u = dependent variable being solved (pressure squared)
c     ui = initial pressure squared values
c     vel = darcy velocity [meter / second]
c     velb = velocity out of borehole [meter / second]
c
      integer n,imax,kf,l
      real mu
      character name*20, input*20, lbc*4, rbc*4, ans
      parameter (n=50, pi=3.14159)
      real a(n), b(n), c(n), r(n), u(n), ui(n), dt, t,
     1 dr,vel(n), epsil, perm, press(n), pressi(n),velb,thick
c
c  Open an input file
c
      write (6,*) 'Enter input file name'
      read (5,*) input
      open (unit = 8,file = input)
      read (8,*) perm,mu,epsil,dt,imax,thick,itran
      read (8,*) lbc,rbc
        if ((lbc .eq. 'pres') .and. (rbc .eq. 'pres')) then
          read (8,*) (pressi(j), j=1,n)
          kf = 2
          l = n-1
        else if ((lbc .eq. 'pres') .and. (rbc .eq. 'flux')) then
          read (8,*) (pressi(j), j=1,n)
          read (8,*) vel(n)
          kf = 2
          l = n
```

```
          else if ((lbc .eq. 'flux') .and. (rbc .eq. 'pres')) then
            read (8,*) (pressi(j),j=1,n)
            read (8,*) vel(1)
            kf = 1
            l = n-1
          else if ((lbc .eq. 'flux') .and. (rbc .eq. 'flux')) then
            read (8,*) (pressi(j), j=1,n)
            read (8,*) vel(1)
            read (8,*) vel(n)
            kf = 1
            l = n
          else
            write (6,*) 'Incorrect Input Format -- Program Halted'
           stop
         endif
         read (8,*) dr
c
c  Open an output file
c
      write (6,*) 'Enter output file name'
      read (5,21) name
   21 format(a)
      open(unit = 9,file = name,status = 'new',err = 17)
      goto 190
   17 write (6,*) 'ERROR: file exists--write over it (y/n)?'
      read (5,21) ans
          if (ans .eq. 'y') then
            open(9,file=name,status='unknown')
          else
            stop
          end if
c
c  Open an output file suitable for time vs. borehole vel data
c
  190 write (6,*) 'Enter file name for time vs. borehole velocity data'
      read (5,21) name
      open(unit = 11,file = name,status = 'new',err = 170)
      goto 500
  170 write (6,*) 'ERROR: file exists--write over it (y/n)?'
      read (5,21) ans
          if (ans .eq. 'y') then
            open(11,file=name,status='unknown')
          else
            stop
          end if
c
c  Open an output file for pressure vs. time data
c
  500 write (6,*) 'Enter file name for pressure vs. distance data'
      read (5,21) name
      open(unit = 12,file = name,status = 'new',err = 171)
      goto 19
  171 write (6,*) 'ERROR: file exists--write over it (y/n)?'
      read (5,21) ans
          if (ans .eq. 'y') then
            open(12,file=name,status='unknown')
```

```
          else
            stop
          end if
c
c  Initialize variables
c
   19   do 2 j=1,n
          ui(j) = pressi(j) ** 2
    2 continue
      t = 0.
      alpha = perm / (epsil * mu)
      if (kf .eq. 2) press(1) = pressi(1)
      if (l .eq. n-1) press(n) = pressi(n)
c
c  Execute main do loop
c
      do 99 i = 1,imax
c
c  Solve right hand column matrix
c
      if (kf .eq. 1) then
      r(1) = -vel(1) * vel(1) * mu * mu * dr * dr /
     1 (perm * perm) + 2. * sqrt(ui(1)) * sqrt(ui(2))
      endif
c
      if (kf .eq. 2) then
      r(2) = (alpha * pressi(1) / (4. * dr * dr) -
     1 alpha * pressi(1) / (2. * dr * dr)) * ui(1) + (alpha *
     2 pressi(2) / (dr * dr) - 1. / dt) * ui(2) - (alpha *
     3 pressi(3) / (2. * dr * dr) + alpha * pressi(3) /
     4 (4. * dr * dr)) * ui(3) - (alpha * pressi(1) / (2. *
     5 dr * dr) - alpha * pressi(1) / (4. * dr * dr)) * ui(1)
      else
      r(2) = (alpha * pressi(1) / (4. * dr *
     1  dr) - alpha * pressi(1) / (2. * dr * dr))
     2  * ui(1) + (alpha * pressi(2) / (dr * dr) -
     3  1. / dt) * ui(2) - (alpha * pressi(3) / (2. * dr *
     4  dr) + alpha * pressi(3) / (4. *
     5  dr * dr)) * ui(3)
      endif
c
      do 81 j = 3,n-2
      r(j) = (alpha * pressi(j-1) / (4. * (j-1) * dr *
     1  dr) - alpha * pressi(j-1) / (2. * dr * dr))
     2  * ui(j-1) + (alpha * pressi(j) / (dr * dr) -
     3  1. / dt) * ui(j) - (alpha * pressi(j+1) / (2. * dr *
     4  dr) + alpha * pressi(j+1) / (4. * (j-1) *
     5  dr * dr)) * ui(j+1)
   81 continue
c
      if (l .eq. n-1) then
      r(n-1) = (alpha * pressi(n-2) / (4. * (n-2) * dr * dr) -
     1 alpha * pressi(n-2) / (2. * dr * dr)) * ui(n-2) + (alpha
     2 * pressi(n-1) / (dr * dr) - 1. / dt) * ui(n-1) - (alpha *
     3 pressi(n) / (2. * dr * dr) + alpha * pressi(n) / (4. *
     4 (n-2) * dr * dr)) * ui(n) - (alpha * pressi(n) / (2. * dr
```

```
     5 * dr) + alpha * pressi(n) / (4. * (n-2) * dr * dr)) *
     6 ui(n)
        else
       r(n-1) = (alpha * pressi(n-2) / (4. * (n-2) * dr *
     1  dr) - alpha * pressi(n-2) / (2. * dr * dr))
     2  * ui(n-2) + (alpha * pressi(n-1) / (dr * dr) -
     3  1. / dt) * ui(n-1) - (alpha * pressi(n) / (2. * dr *
     4  dr) + alpha * pressi(n) / (4. * (n-2) *
     5  dr * dr)) * ui(n)
        endif
c
c      endif
c
      if (1 .eq. n) then
      r(n) = vel(n) * vel(n) * mu * mu * dr * dr /
     1 (perm * perm) + 2. * sqrt(ui(n-1)) * sqrt(ui(n))
      endif
c
c  Solve subdiagonal vector of coefficient matrix
c
      do 11 j=2,n-1
          a(j) = (alpha * pressi(j-1) / (2. * dr * dr) -
     1     alpha * pressi(j-1) / (4. * (j-1) * dr * dr))
   11 continue
      a(n) = 1.
c
c  Solve superdiagonal vector of coefficient matrix
c
      c(1) = 1.
      do 12 j=2,n-1
          c(j) =(alpha * pressi(j+1) / (2. * dr * dr) + alpha *
     1    pressi(j+1) / (4. * (j-1) * dr * dr))
   12 continue
c
c  Solve diagonal vector of coefficient matrix
c
      do 15 j = 2,n-1
          b(j) = -(alpha * pressi(j) / (dr * dr) + 1. / dt)
   15 continue
      b(1) = 1.
      b(n) = 1.
c
c  Call the tridiagonal matrix solver
c
          call tridag (a,b,c,r,u,n,kf,1)
c
c  Compute pressures from u vector
c
      if (kf .eq. 1) then
        press(1) = sqrt(u(1))
      endif
      do 20 j = 2,n-1
          press(j) = sqrt(u(j))
   20 continue
      if (1 .eq. n) then
        press(n) = sqrt(u(n))
```

```
      endif
c
c  Compute Darcy velocities
c
      do 25 j=2,n-1
        vel(j) = -perm / (mu * dr) * (press(j) - press(j-1))
   25   continue
c
c  If either boundary is prescribed pressure, flux will change
c  and must be updated
c
       if (kf .eq. 2) then
         vel(1) = -perm / (mu * dr) * (press(2) - press(1))
       endif
       if (l .eq. n-1) then
         vel(n) = -perm / (mu * dr) * (press(n) - press(n-1))
       endif
c
c  Compute velocity out of borehole
c
       velb = -2. * vel(1) * thick / (epsil * dr)
c
c  Call output to write results to screen
c
c     call output(dt,t,press,n,vel,velb)
c
c  The following is for transient bc's at the borehole.  If the pressure
c  changes, its value needs to be 'helped' along through the program,
c  otherwise tridag will recognize the initial value at the boundary.
c
      if (itran .eq. 1) press(1) = pressi(1)
c
c  Write results to separate file
c
        if (i .eq. imax) then
      write (9,58) dt + t
   58 format (1x,'The time is ', e10.5,' seconds'/)
      write (9,61) velb
   61 format (1x,'The velocity at the borehole is ',e10.4, ' meters
     1 per second')
      write (9,60) n
   60 format (1x,//,'List of pressures for', i3,'  nodes:'/
     1 1x, 30('='))
      write (9,65) (press(j), j=1,n)
   65 format (1x,e15.4)
      write (9,70) n
   70 format (//,1x,'List of velocities for',i3, '  nodes:'/
     1 1x, 31('='))
      write (9,75) (vel(j), j=1,n)
   75 format (1x,e15.4)
      write (9,77)
   77 format (1x,31('*'),//)
      endif
c
c  Write time and borehole velocity to separate file
c
```

```
      days = (dt + t) / 86400.
      write (11,101) days,velb
  101 format (1x,e15.6,1x,e10.4)
c
c  Write distance and pressures to separate file, at last time
c  step
c
      if (i .eq. imax) then
      write (12,201) 0.,pressi(1)
  201 format (1x,e10.4,3x,e10.4)
      do 302 j=1,n-2
        write (12,201) j * dr, press(j+1)
  302 continue
      write (12,201)  (n-1) * dr,pressi(n)
      endif
c
c  If the pressure change is less than 1% at the left hand
c  boundary, jump out of loop
c
c     if ((ui(1) / u(1) .lt. .01) .or. u(1) / ui(1) .lt. .01)
c    1 goto 50
c
c  If either boundary condition is to be updated, call bound
c
       call bound(n,ui,pressi,dt,t)
c
c  Update dependent variables, ui and pressi
c
      do 55 j=2,n-1
          pressi(j) = press(j)
          ui(j) = u(j)
   55 continue
      if (kf .eq. 1) then
        pressi(1) = press(1)
        ui(1) = u(1)
      endif
      if (l .eq. n) then
        pressi(n) = press(n)
        ui(n) = u(n)
      endif
c
c  Increment time step
c
      t = t + dt
   99 continue
c
      close(8)
      close(9)
      close(11)
      close(12)
   50 stop
      end
c
      subroutine bound(n,ui,pressi,dt,t)
      dimension ui(n), pressi(n)
      real period,dt,t,pi,amp
```

```
      integer n
c     amp = 200.
      amp = 400.
      pi = 3.14159265
      period = 8.64e+04
c  Enter function here
      pressi(1) = 100000. + amp * sin(2. * pi * (dt + t) / period)
c     pressi(50) = 100000. - amp * sin(2. * pi * (dt + t) / period)
      ui(1) = pressi(1) * pressi(1)
c     ui(50) = pressi(50) * pressi(50)
      return
      end
c
      subroutine output(dt,t,press,n,vel,velb)
      integer n
      real press(n),vel(n),dt,t
      write (6,32) dt + t
   32 format (1x,'The time is ', e10.5,' seconds'/)
      write (6,31) velb
   31 format (1x,'The velocity at the borehole is ',e10.4, ' meters
     1 per second')
      write (6,30) n
   30 format (1x,//,'list of pressures for', i3,' nodes:'/
     1 1x, 30('='))
      write (6,35) (press(j), j=1,n)
   35 format (1x,e15.4)
      write (6,40) n
   40 format (//,1x,'list of velocities for',i3, ' nodes:'/
     1 1x, 31('='))
      write (6,45) (vel(j), j=1,n)
   45 format (1x,e15.4)
      write (6,47)
   47 format (1x,31('*'),//)
      return
      end
c
c  Subroutine for solving a system of linear simultaneous
c  equations having a tridiagonal coefficient matrix.
c  The equations are numbered from kf through l, and their
c  subdiagonal, diagonal, and superdiagonal coefficients are
c  stored in the arrays a, b, and c.  The computed solution vector
c  v(kf)...v(l) is stored in the array v.
c
      subroutine tridag(a,b,c,d,v,n,kf,l)
      dimension a(n), b(n), c(n), d(n), v(n), beta(101),
     1 gamma(101)
c
      beta(kf) = b(kf)
      gamma(kf) = d(kf) / beta(kf)
      kfpl = kf + 1
      do 1 j = kfpl, l
        beta(j) = b(j) - a(j) * c(j-1) / beta(j-1)
        gamma(j) = (d(j) - a(j) * gamma(j-1)) / beta(j)
    1 continue
c
      v(l) = gamma(l)
```

```
      last = l - kf
      do 2 k=1,last
        i = l - k
        v(i) = gamma(i) - c(i) * v(i+1) / beta(i)
    2 continue
      return
      end
```

APPENDIX C

```
      SUBROUTINE RELP(SG,REPL,REPG,NMAT,K,NLOC,SG0)
      include "file.double"
C
C-----THIS ROUTINE COMPUTES RELATIVE PERMEABILITIES FOR LIQUID
C     AND GASEOUS PHASES.
c
      dimension fracn(27),totn(27)
C
      COMMON/P3/DELX(1)
      COMMON/RPCAP/IRP(27),RP(7,27),ICP(27),CP(7,27),IRPD,RPD(7),
     1  ICPD,CPD(7)
C
      data fracn/.0018,.0028,25*0./
      data totn/.0668,.1028,25*0./
c
      SL=1.-SG
c     GO TO (10,11,12,12,13,14,15,16),IRP(NMAT)
      goto (10,11,12,12,13,14,15,16,17),irp(nmat)
   10 CONTINUE
C-----LINEAR FUNCTIONS.
C
C     CHECK IF INCREMENT NEEDS TO BE ADJUSTED AT LOWER LIQUID CUTOFF.
      IF (K.NE.3) GO TO 20
      IF ((SL-RP(1,NMAT))*(1.-SG0-RP(1,NMAT)).GE.0.) GO TO 20
C     ADJUST INCREMENT.
      DELX(NLOC+2)=-DELX(NLOC+2)
      SG=SG0+DELX(NLOC+2)
      SL=1.-SG
   20 CONTINUE
      REPL=(SL-RP(1,NMAT))/(RP(3,NMAT)-RP(1,NMAT))
      IF (SL.GE.RP(3,NMAT)) REPL=1.
      IF (SL.LE.RP(1,NMAT)) REPL=0.
      REPG=(SG-RP(2,NMAT))/(RP(4,NMAT)-RP(2,NMAT))
      IF (SG.GE.RP(4,NMAT)) REPG=1.
      IF (SG.LE.RP(2,NMAT)) REPG=0.
      RETURN
C
   11 CONTINUE
C-----RELATIVE PERMEABILITY OF PICKENS ET AL.
C
      REPG=1.
      REPL=(1.-SG)**RP(1,NMAT)
C
      RETURN
C
   12 CONTINUE
C-----COREY'S OR GRANT'S CURVES.
C
      SSTAR=(SL-RP(1,NMAT))/(1.-RP(1,NMAT)-RP(2,NMAT))
      REPL=SSTAR**4
      REPG=(1.-SSTAR**2)*(1.-SSTAR)**2
      IF (SG.GE.RP(2,NMAT)) GO TO 50
      REPG=0.
      REPL=1.
      GO TO 102
   50 IF (SG.LT.(1.-RP(1,NMAT))) GO TO 102
```

```
      REPL=0.
      REPG=1.
  102 CONTINUE
      IF (IRP(NMAT).EQ.4) REPG=1.-REPL
      RETURN
C
   13 CONTINUE
C-----BOTH PHASES ARE PERFECTLY MOBILE.
C
      REPL=1.
      REPG=1.
C
      RETURN
   14 CONTINUE
C-----RELATIVE PERMEABILITIES OF FATT AND KLIKOFF (1959), AS REPORTED
C     BY K. UDELL (BERKELEY, 1982).
C
      SS=0.
      IF (SL.GT.RP(1,NMAT)) SS=(SL-RP(1,NMAT))/(1.-RP(1,NMAT))
      REPL=SS**3
      REPG=(1.-SS)**3
      RETURN
C
C
   15 CONTINUE
C-----RELATIVE PERMEABILITY OF VAN GENUCHTEN, SOIL SCI. SOC. AM. J. 44,
C     PP. 892-898, 1980.
C
      IF (SL.GE.RP(3,NMAT)) GO TO 150
      SS=(SL-RP(2,NMAT))/(RP(3,NMAT)-RP(2,NMAT))
      REPL=0.
      IF (SS.GT.0.)
     1   REPL=SQRT(SS)*(1.-(1.-SS**(1./RP(1,NMAT)))**RP(1,NMAT))**2
      REPG=1.-REPL
      RETURN
C
  150 REPL=1.
      REPG=0.
      RETURN
C
   16 CONTINUE
C     RELATIVE PERMEABILITIES AS MEASURED BY VERMA ET AL. IN
C     LABORATORY FLOW EXPERIMENTS FOR STEAM-WATER MIXTURES
C
      SS=(SL-RP(1,NMAT))/(RP(2,NMAT)-RP(1,NMAT))
      IF(SS.GT.1.) SS=1.
      IF(SS.LT.0.) SS=0.
      REPL=SS**3
      REPG=RP(3,NMAT)+RP(4,NMAT)*SS+RP(5,NMAT)*SS*SS
      IF(REPG.GT.1.) REPG=1.
      IF(REPG.LT.0.) REPG=0.
      RETURN
C
   17 continue
c---- Relative permeability of van Genuchten, but modified for
c     an equivalent porous medium after K. Pruess and J.S.Y. Wang,
```

```
c     1987, "Numerical modeling of isothermal and nonisothermal
c     flow in unsaturated fractured rock -- a review," in AGU
c     Monograph 42, Flow and Transport Through Unsaturated
c     Fractured Rock, edited by Daniel D. Evans and Thomas J. Nicholson,
c     pp. 11-21.
c
c             Clay A. Cooper    May, 1989
c
c     To Use:  Include rp(1) through rp(7) in the input file.  Change
c     the data statements at the top of this subroutine for the
c     correct fracture and total porosities of each material
c     property.
c
c     rp(1)  = matrix permeability
c     rp(2)  = fracture permeability
c     rp(3)  = van Genuchten's lambda for matrix
c     rp(4)  = van Genuchten's lambda for fractures
c     rp(5)  = "critical saturation" -- matrix porosity / total porosity
c     rp(6)  = residual liquid saturation of matrix
c     rp(7)  = critical moisture content (similar to rp(5))
c     sl     = liquid saturation
c     ssm    = effective liquid saturation of matrix
c     ssf    = effective liquid saturation of fractures
c     srf    = residual liquid saturation of fractures
c     sssf   = saturation cutoff value above which fractures are sat.
c     rpliqm = liquid relative permeability of the matrix
c     rpliqf = liquid relative permeability of the fractures
c     repl   = equivalent porous medium liquid relative permeability
c     repg   = equivalent porous medium gas relative permeability
c
c     fracn  = fracture porosity
c     totn   = total porosity
c     nmat   = material number chosen internally by TOUGH
c
      if (sl .lt. rp(6,nmat)) then
        repl = 0.
        repg = 1.
      endif
c
      if (sl .lt. rp(5,nmat) .and. sl .ge. rp(6,nmat))  then
        ssm = (sl - rp(6,nmat)) / (rp(5,nmat) - rp(6,nmat))
        rpliqm = sqrt(ssm)*(1.-(1.-ssm**(1./rp(3,nmat)))**rp(3,nmat))**2
        rpliqf = 0.
        repl = (rp(1,nmat) * rpliqm + rp(2,nmat) * rpliqf) /
     1    (rp(1,nmat) + rp(2,nmat))
        repg = 1. - repl
      endif
c
      if (sl .ge. rp(5,nmat) .and. sl .lt. 1.) then
        ssm = 1.
        rpliqm=sqrt(ssm)*(1.-(1.-ssm**(1./rp(3,nmat)))**rp(3,nmat))**2
c
        amoist = sl * totn(nmat)
        templ = amoist - rp(7,nmat)
        ssf = templ / fracn(nmat)
        rpliqf=sqrt(ssf)*(1.-(1.-ssf**(1./rp(4,nmat)))**rp(4,nmat))**2
```

```
c
        repl = (rp(1,nmat) * rpliqm + rp(2,nmat) * rpliqf) /
     1   (rp(1,nmat) + rp(2,nmat))
        repg = 1. - repl
      endif
c
      if (sl .eq. 1.) then
        repl = 1.
        repg = 0.
      endif
      return
c
      end
```